

Leading twist T -even TMDs for the spin-1 heavy vector mesons

Satyajit Puhan^{*} and Harleen Dahiya[†]

Department of Physics, Dr. B.R. Ambedkar National Institute of Technology, Jalandhar, 144008, India

 (Received 24 July 2023; accepted 30 December 2023; published 5 February 2024)

We have presented the leading twist quark transverse momentum-dependent parton distribution functions (TMDs) for the spin-1 heavy vector mesons J/ψ -meson and Υ -meson using the overlap of the light-front wave functions. We have computed their TMDs in the light-front holographic model (LFHM) as well as the light-front quark model (LFQM) and further compared the results with the Bethe-Salpeter (BSE) model. We have discussed the behavior of the TMDs with respect to momentum fraction carried by active quark (x) and the transverse quark momenta (k_{\perp}) in both the models. We have also calculated the k_{\perp} moments of the quark in both the models and have compared the results with the BSE model. The predictions of LFQM are found to be in accord with the BSE model. Further, we have analyzed the leading twist parton distribution functions (PDFs) for both the heavy mesons in both the models and the results are found to be in accord with the basic light-front quantization (BLFQ) and BSE model.

DOI: [10.1103/PhysRevD.109.034005](https://doi.org/10.1103/PhysRevD.109.034005)

I. INTRODUCTION

Hadrons, which are strongly interacting and relativistic bound states of quarks and gluons, have a complex structure. An important goal of both theoretical and experimental physicists is to understand the hadron structure in terms of the theory of strong interactions: quantum chromodynamics (QCD) [1–3] and the hadronic matrix elements of quark-gluon field operators. Even though the parton distribution functions (PDFs) [4–7], extracted from the deep inelastic scattering (DIS) [8] experiments, provide information about the longitudinal momentum fraction (x) distribution of the quarks, they do not specify the spatial location, transverse momentum distribution and spin densities of the quarks inside the hadrons. Further, the three-dimensional transverse momentum-dependent parton distributions (TMDs) [9–12] and the generalized parton distributions (GPDs) [13–15] play an important role in describing a complete internal structure of the hadron. Both TMDs and GPDs are widely investigated experimentally as well as theoretically in these recent years. GPDs are a function of longitudinal momentum fraction of parton (x) as well as momentum transferred fraction (Δ) between initial and final state of a hadron.

It contains information about spatial distribution of the partons inside a hadron which cannot be accessed through TMDs. GPDs can be accessed through the deeply virtual Compton scattering (DVCS) [16] and deeply virtual meson production (DVMP) [17,18] processes. On the other hand, TMDs contain information about both the longitudinal momentum fraction (x) and transverse momentum distribution (k_{\perp}) of the partons inside a hadron. TMDs also provide nonperturbative information about parton structure of hadrons, particularly angular momentum, spin-orbit correlation and polarization degrees of freedom for the partons inside a hadron [19]. The extended form of co-linear PDFs gives rise to the three-dimensional TMDs. Experimentally, TMDs can be extracted from deep inelastic scattering (DIS) processes at high energy [8], Drell-Yan processes [20–24], semi-inclusive deep inelastic scattering (SIDIS) processes [25–27], and Z^0/W^{\pm} production [28–30].

A wide range of theoretical studies are going on to study the TMDs of hadrons. For the case of nucleons which are spin- $\frac{1}{2}$ particles, TMDs have been studied at the leading twist in different QCD-inspired models like light-front constituent quark model (LFCQM) [31], quark-diquark model [32], chiral quark soliton model [33], bag model [34] and lattice QCD [35]. A few higher twist TMDs calculations for the nucleons have also been done [36,37]. There are in total eight TMDs for the case of spin- $\frac{1}{2}$ particles out of which six are T-even at leading twist [38]. TMDs have also been calculated for the case of spin-0 light mesons at the leading twist [39–41] and also for spin-1 light mesons at the leading twist [42,43]. There are only two TMDs at leading twist for the case of spin-0 mesons [44] whereas there are eighteen TMDs for the case of spin-1 vector

^{*}puhansatyajit@gmail.com

[†]dahiyah@nitj.ac.in

Published by the American Physical Society under the terms of the Creative Commons Attribution 4.0 International license. Further distribution of this work must maintain attribution to the author(s) and the published article's title, journal citation, and DOI. Funded by SCOAP³.

mesons at lower twist out of which nine are T -even [45]. Three tensor polarized TMDs $f_{1LL}(x, \mathbf{k}_\perp^2)$, $f_{1LT}(x, \mathbf{k}_\perp^2)$ and $f_{1TT}(x, \mathbf{k}_\perp^2)$ come into the picture in the case of spin-1 particles. These TMDs occur due to the tensor polarizations of the target and are absent in case of spin-0 pseudoscalar mesons and spin- $\frac{1}{2}$ nucleons. For the case of spin-1 hadron, there is an extra tensor PDF $f_{1LL}(x)$ when compared with the spin-0, $\frac{1}{2}$ targets.

At present, there is no experimental data available for extracting the spin-1 meson TMDs but a very few theoretical predictions are available. Spin-1 TMDs and TMD fragmentation functions have been predicted at the leading twist as well as at higher twist with positivity bounds on them [45]. Detailed investigations on the ρ meson T -even TMDs along with PDFs have been carried out in the Nambu-Jona-Lasinio (NJL) model [46], light-front quark model (LFQM) [43], light-front holographic model (LFHM) [43] and BSE model [42]. Photon TMDs have been studied in the basic light-front quantization (BLFQ) method [47]. All these models successfully encode the TMDs, PDFs, and TMD fragmentation functions for the light vector mesons. There are however very few investigations on the heavy vector mesons like J/ψ and Υ . In the BLFQ method, the study of the heavy vector mesons PDFs have been done for the case of quark being unpolarized [48]. A detailed study of all the PDFs for J/ψ has been performed using the light-front wave functions (LFWFs) method [49,50]. An overview of the TMDs and PDFs for spin-1 mesons has been presented in BSE model [42], however, there is no mention of $f_{1LL}(x)$ PDF, $f_{1LL}(x, \mathbf{k}_\perp^2)$ TMDs for both J/ψ and Υ particles in this work. The J/ψ and Υ mesons get their masses from the current quark mass through the Higgs mechanism. The parton's motion inside J/ψ is slower as compared to the other vector mesons making the motion nonrelativistic. The motion of parton in Υ is even slower than J/ψ meson hence providing a benchmark for TMDs in the non-relativistic limit. Following the success of the LFHM as well as LFQM in predicting the results for ρ -mesons and in light of the above developments, a detailed study of J/ψ and Υ mesons would be interesting in order to understand the three-dimensional structure of the heavy vector mesons.

In this work, we have mainly targeted the quark distributions of J/ψ and Υ heavy vector mesons using the light-front (LF) dynamics based LFHM and LFQM. The LFQM is a nonperturbative approach framework describing the structure and dynamics of hadrons as well as the behavior of quarks within them [51–58]. LFQM is relativistic and gauge invariant in nature. The advantage of LFQM is that it focuses on the valence quarks of the hadrons and the valence quarks are the primary constituents responsible for the overall structure and properties of

hadrons. At times, LFQM can describe the hadrons in the strong interaction regime when the perturbative QCD calculations cannot. However, higher Fock-state contributions and effect of confinement, which play an important role to describe the complete dynamics of hadrons, are not included in LFQM. LFQM describes the structure only in the lower Fock-states. Further, the LFHM goes beyond the simple picture of constituent quarks and gluons by considering the full holographic dual description. LFHM relates the higher dimensional gravitational theory to lower dimensional quantum field theory for strongly interacting systems [59–61].

In the present work, we have proceeded through both the LFQM and LFHM to calculate the T -even TMDs for J/ψ and Υ mesons. We have obtained the explicit forms of the quark TMDs in the overlapping form of LFWFs in both the models. We have taken the lower Fock-state for these particles, i.e., $|M\rangle = \sum |q\bar{q}\rangle\psi_{q\bar{q}}$ as there is very less contribution from higher Fock-states for the heavy mesons. In the LFQM, the tensor TMDs $f_{1LL}(x, \mathbf{k}_\perp^2)$, $f_{1LT}(x, \mathbf{k}_\perp^2)$, and $f_{1TT}(x, \mathbf{k}_\perp^2)$ come out to be zero. Whereas, $h_{1T}^+(x, \mathbf{k}_\perp^2)$ TMD is zero in the LFHM. We have discussed the TMDs in both models with the help of three-dimensional and two-dimensional plots with respect to x and \mathbf{k}_\perp^2 . We have calculated average quark transverse momenta \mathbf{k}_\perp^2 for both the models and compared the results with the BSE model [42] as no experimental data is available. The PDFs have also been computed for both the models and have been compared with the results from the BLFQ [48], designed light-front wave functions (D-LFWF) [49] and BSE Model [42].

This paper is arranged as follows. In Sec. II A, we have defined the leading twist TMDs and the correlation functions for the spin-1 hadrons at lower Fock-state. In Secs. II B and II C, the essential details of the LFHM and LFQM have respectively been presented. Further in Sec. II D, the basic formalism of LFWFs has been given. We represent different TMDs in the form of light-front amplitude with their explicit overlap form in both the models. In Sec. II E, we have given the details of the numerical results with the help of three-dimensional and two-dimensional plots. We have also compared our results with other model results in this section. In Sec. III, we have discussed the collinear PDFs. Finally, we summarize our results in Sec. IV.

II. METHODOLOGY

A. Transverse momentum-dependent parton distributions

The quark TMDs for spin-1 particles are defined through transverse momentum-dependent quark correlation function expressed as [22,46,62–66]

$$\begin{aligned}\Theta_{ij}^{(\Lambda)S}(x, \mathbf{k}_\perp^2) &= \int \frac{dz^- d^2 \mathbf{z}_\perp}{(2\pi)^3} e^{i(k^+ z^- - k_\perp \cdot z_\perp)} \mathcal{S} \langle P, \Lambda | \bar{\psi}_j(0) W(0, z) \psi_i(z^-, \mathbf{z}_\perp) | P, \Lambda \rangle_{\mathcal{S}} \\ &\equiv \epsilon_{\Lambda(\mu)}^*(P) \Theta_{ij}^{\mu\nu}(x, \mathbf{k}_\perp) \epsilon_{\Lambda(\nu)}(P),\end{aligned}\quad (1)$$

where $\psi_{i(j)}$ is the flavor SU(2) quark field operator, i and j are the Dirac indices, and $W(0, z)$ is the gauge link [65,66]. For simplicity, we have taken the gauge link as unity to study the T -even TMDs. P is the four-vector momentum of heavy vector mesons and is expressed as

$$P = (P^+, P^-, \mathbf{P}_\perp) = \left(P^+, \frac{M_\alpha}{P^+}, \mathbf{0}_\perp \right),$$

where M_α is the mass for heavy vector meson. $M_\alpha = M_{c\bar{c}}$ and $M_\alpha = M_{b\bar{b}}$ for J/ψ meson and Υ meson respectively.

k_\perp and k^+ are transverse and longitudinal momentum carried by the active quark, z is the position four vector and is expressed as, $z = (z^+, z^-, z_\perp)$ in LF dynamics. In Eq. (1), $\Theta_{ij}^{\mu\nu}$ is the polarization-independent Lorentz tensor matrix, $\epsilon_{\mu(\nu)}$ is the polarization four vector and the $|P, \Lambda\rangle_{\mathcal{S}}$ state indicates that the spin projection of the target hadron in $S = (S_L, S_T)$ direction with helicities $\Lambda = \pm 1, 0$. At the leading twist, there are total nine T -even TMDs for J/ψ and Υ which are expressed with unpolarized (U), transversely polarized (T) and longitudinally polarized (L) target as

$$\epsilon_{\Lambda(\mu)}^*(P) \langle \gamma^+ \rangle_S^{\mu\nu}(x, \mathbf{k}_\perp^2) \epsilon_{\Lambda(\nu)}(P) = f_1(x, \vec{k}_\perp^2) + S_{LL} f_{1LL}(x, \vec{k}_\perp^2) + \frac{\vec{S}_{LT} \cdot \vec{k}_\perp}{M_\alpha} f_{1LT}(x, \vec{k}_\perp^2) + \frac{\vec{S}_{TT} \cdot \vec{k}_\perp}{M_\alpha^2} f_{1TT}(x, \vec{k}_\perp^2), \quad (2)$$

$$\epsilon_{\Lambda(\mu)}^*(P) \langle \gamma^+ \gamma_5 \rangle_S^{\mu\nu}(x, \mathbf{k}_\perp^2) \epsilon_{\Lambda(\nu)}(P) = S_L g_{1L}(x, \mathbf{k}_\perp^2) + \frac{\mathbf{k}_\perp \cdot \mathcal{S}_\perp}{M_\alpha} g_{1T}(x, \mathbf{k}_\perp^2), \quad (3)$$

$$\epsilon_{\Lambda(\mu)}^*(P) \langle \gamma^+ \gamma^i \gamma_5 \rangle_S^{\mu\nu}(x, \mathbf{k}_\perp^2) \epsilon_{\Lambda(\nu)}(P) = S_\perp^i h_1(x, \mathbf{k}_\perp^2) + S_L \frac{k_\perp^i}{M_\alpha} h_{1L}^+(x, \mathbf{k}_\perp^2) + \frac{1}{2M_\alpha^2} (2k_\perp^i \mathbf{k}_\perp \cdot \mathcal{S}_\perp - S_\perp^i \mathbf{k}_\perp^2) h_{1T}^+(x, \mathbf{k}_\perp^2), \quad (4)$$

with

$$\begin{aligned}S_{LL} &= (3\Lambda^2 - 2) \left(\frac{1}{6} - \frac{1}{2} S_L^2 \right), \\ S_{LT}^i &= (3\Lambda^2 - 2) S_L S_\perp^i, \\ S_{TT}^{ij} &= (3\Lambda^2 - 2) \left(S_\perp^i S_\perp^j - \frac{1}{2} S_\perp^2 \delta^{ij} \right).\end{aligned}$$

The Lorenz tensor is defined as

$$\epsilon_{\Lambda(\mu)}^*(P) \langle \Gamma \rangle^{\mu\nu}(x, \mathbf{k}_\perp^2) \epsilon_{\Lambda(\nu)}(P) = \frac{1}{2} \text{Tr}_D(\Gamma \Theta^{(\Lambda)S}(x, \mathbf{k}_\perp^2)).$$

In the above equations $S_\perp^{i(j)}$ symbolize the transverse polarization of the target meson in the directions $i(j)$ or $x(y)$. The Dirac matrices structure Γ for leading twist are γ^+ , $\gamma^+ \gamma_5$ and $\gamma^+ \gamma^i \gamma_5$ with $i = (1, 2)$. The function f , g and h denote the unpolarized, longitudinally polarized and transversely polarized quark within the hadron. The subscript 1 in the functions f , g , h [Eqs. (2)–(4)] denotes the leading twist TMDs [45]. The longitudinal and transverse hadron polarizations have been denoted as L and T respectively. x in the above equations is the momentum fraction carried by the active quark from the target hadron i.e., $x = \frac{k^+}{P^+}$.

When compared with the spin- $\frac{1}{2}$ case of nucleons, the spin-1 hadrons have three extra tensor polarized TMD functions f_{1LT} , S_{LT} and f_{1TT} .

B. Light-front holographic model

LFHM is derived from the AdS/QCD correspondence which connects the five-dimensional Anti-de Sitter (AdS) space-time to the lower dimension QCD in the LF dynamics [43,59,67]. In the LFHM, hadrons are described by string-like objects in the higher dimensional AdS space. The behavior of these strings corresponds to the confinement of quarks and gluons within the hadrons. The complete holographic wave function $\psi^{(1)}(x, \zeta, \varphi)$ is expressed as [67–69]

$$\psi^{(1)}(x, \zeta, \varphi) = \frac{\Phi(\zeta)}{\sqrt{2\pi\zeta}} X(x) e^{iL\varphi}, \quad (5)$$

where $X(x)$ is the longitudinal mode of LFWF and can be written as $X(x) = \sqrt{x(1-x)}$ [67], φ is the transverse angular dependence in light-front plane, $\zeta = X(x)b_\perp$ is a light-front variable and b_\perp is the transverse quark pair separation variable in the hadrons. The dynamic part of the

holographic wave function, derived from the holographic Schrödinger equation [43], is expressed as

$$\Phi_{nL}(\zeta) = \kappa^{1+L} \sqrt{\frac{2n!}{(n+L)!}} \zeta^{1/2+L} \exp\left(\frac{-\kappa^2 \zeta^2}{2}\right) L_n^L(\kappa^2 \zeta^2), \quad (6)$$

with meson mass spectrum

$$M^2 = (4n + 2L + 2)\kappa^2 + 2\kappa^2(J - 1), \quad (7)$$

where κ is the mass scale parameter and its value is 0.894 GeV and 1.49 GeV for $J/\psi(c\bar{c})$ [70] and $\Upsilon(b\bar{b})$ [71] respectively. n , J , and L are the radial quantum number, total angular momentum, and internal angular momentum, respectively. We can get the ground state holographic wave function from Eq. (5) in the transverse impact-parameter space as

$$\psi^{(1)}(x, \zeta^2) = \frac{\kappa}{\sqrt{\pi}} \sqrt{x(1-x)} \exp\left(\frac{-\kappa^2 \zeta^2}{2}\right). \quad (8)$$

By Fourier transforming Eq. (8), we obtain the wave function for the mesons with massless quarks in transverse momentum space

$$\psi^{(1)}(x, \mathbf{k}_\perp^2) \propto \frac{1}{\sqrt{x(1-x)}} \exp\left(-\frac{M^2}{2\kappa^2}\right). \quad (9)$$

Here M is the meson invariant mass which is given as

$$M^2 = \frac{\mathbf{k}_\perp^2}{x(1-x)},$$

where k_\perp is the transverse quark momentum obtained by taking Fourier transform of b_\perp . Since we are dealing with the massive quarks, we can include the quark mass in the invariant mass form [72,73]. We have

$$M_{q\bar{q}}^2 = \frac{\mathbf{k}_\perp^2}{x(1-x)} + \frac{m_q^2}{x} + \frac{m_{\bar{q}}^2}{1-x}, \quad (10)$$

where m_q and $m_{\bar{q}}$ are the quark and antiquark mass respectively. Now the holographic light-front wave function for meson bound state in Eq. (9) with quark masses is modified as

$$\psi^{(1)}(x, \mathbf{k}_\perp^2) \propto \frac{1}{\sqrt{x(1-x)}} \exp\left(-\frac{\mathbf{k}_\perp^2}{2\kappa^2 x(1-x)}\right) \exp\left(-\frac{\mu_{12}^2}{2\kappa^2}\right), \quad (11)$$

where $\mu_{12}^2 = \frac{m_{\bar{q}}^2}{x} + \frac{m_q^2}{1-x}$. The wave function in Eq. (11) has an additional term corresponding to quark masses when

compared to Eq. (9). It would be important to mention here that this is not a solution of the Schrödinger equation for the holographic model, however, the results outcome of the model are more precise by taking the mass term. The holographic wave function in Eq. (11) has been used in the study of ρ meson [43], ρ meson electroproduction at HERA [69] in the decays $B \rightarrow \rho\gamma$ [74], $B \rightarrow K^*$ [75], $B \rightarrow \rho$ [76], $B \rightarrow K^*\mu^-\mu^+$ [77] etc.

For heavy vector mesons $J/\psi(\Upsilon)$, $m_q = (m_c, m_b)$ and $m_{\bar{q}} = (m_{\bar{c}}, m_{\bar{b}})$ denote the masses of quark and antiquarks respectively. As $m_q = m_{\bar{q}}$, so we can rewrite Eq. (11) as

$$\psi^{(1)}(x, \mathbf{k}_\perp^2) \propto \frac{1}{\sqrt{x(1-x)}} \exp\left(-\frac{\mathbf{k}_\perp^2 + m_q^2}{2\kappa^2 x(1-x)}\right). \quad (12)$$

In our work, we have neglected the small contribution coming from the massive quark mass shift following Ref. [43]. The complete wave function is obtained by adding the quark and antiquark helicities with transverse and longitudinal spin projection in the hadrons which are expressed as

$$\chi_{h_q, h_{\bar{q}}}^{(1)L} = \frac{1}{\sqrt{2}} \delta_{h_q, -h_{\bar{q}}}; \quad \chi_{h_q, h_{\bar{q}}}^{(1)T(\pm)} = \frac{1}{\sqrt{2}} \delta_{h_q \pm, h_{\bar{q}} \pm}. \quad (13)$$

In Eq. (13), h_q and $h_{\bar{q}}$ are the helicities of quark and antiquark respectively. Equation (13) can be written in the form of Lorentz invariant spin structure for spin-1 meson by using the photon quark-antiquark vertex factor

$$\chi_{h_q, h_{\bar{q}}}^{(1)L(T)}(x, \mathbf{k}_\perp^2) = \frac{\bar{u}_{h_q}(k^+, \mathbf{k}_\perp)}{\sqrt{x}} \epsilon_\Lambda \cdot \gamma \frac{v_{h_{\bar{q}}}(k'^+, \mathbf{k}'_\perp)}{\sqrt{1-x}}, \quad (14)$$

where k and k' are the quark and antiquark four vector momentum. x and $1-x$ are the longitudinal momentum fraction carried by the quark and antiquark from the hadron, i.e., $x = \frac{k^+}{P^+}$ and $(1-x) = \frac{k'^+}{P^+}$ and the kinematics for polarization vector ϵ_Λ is given as follows

$$\epsilon_L = \left(\frac{P^+}{M_\alpha}, -\frac{M_\alpha}{P^+}, 0, 0\right); \quad \epsilon_T^\pm = \mp \frac{1}{\sqrt{2}}(0, 0, 1, \pm i). \quad (15)$$

The holographic wave function with dynamical spin effects in the longitudinal and transverse spin projection for J/ψ and Υ -mesons can now be written as [69,78]

$$\Psi_{h_q, h_{\bar{q}}}^{(1)L}(x, \mathbf{k}_\perp^2) = \chi_{h_q, h_{\bar{q}}}^{(1)L}(x, \mathbf{k}_\perp^2) \psi^{(1)}(x, \mathbf{k}_\perp^2), \quad (16)$$

$$\Psi_{h_q, h_{\bar{q}}}^{(1)T}(x, \mathbf{k}_\perp^2) = \chi_{h_q, h_{\bar{q}}}^{(1)T}(x, \mathbf{k}_\perp^2) \psi^{(1)}(x, \mathbf{k}_\perp^2). \quad (17)$$

The explicit form of Eqs. (16) and (17) at the model scale $\mu_{\text{LFHM}}^2 = 0.20 \text{ GeV}^2$ are respectively expressed as

$$\Psi_{h_q, h_{\bar{q}}}^{(1)L}(x, \mathbf{k}_{\perp}^2) = \mathcal{N}_L \delta_{h_q, h_{\bar{q}}} \left[M_{\alpha}^2 + \left(\frac{m_q^2 + k_{\perp}^2}{x(1-x)} \right) \right] \psi^{(1)}(x, \mathbf{k}_{\perp}^2), \quad (18)$$

$$\Psi_{h_q, h_{\bar{q}}}^{(1)(T\pm)}(x, \mathbf{k}_{\perp}^2) = \mathcal{N}_T \left[\pm k_{\perp} e^{\pm i\theta_{k_{\perp}}} \left(\frac{\delta_{h_q, \pm} \delta_{h_{\bar{q}}, \mp}}{1-x} - \frac{\delta_{h_q, \mp} \delta_{h_{\bar{q}}, \pm}}{x} \right) + \left(\frac{m_q}{x(1-x)} \right) \delta_{h_q, \pm} \delta_{h_{\bar{q}}, \pm} \right] \psi^{(1)}(x, \mathbf{k}_{\perp}^2), \quad (19)$$

where \mathcal{N}_L and \mathcal{N}_T are the normalization constants and depending on the polarization of the particles they can be computed using

$$\sum_{h_q, h_{\bar{q}}} \int \frac{dx d^2\mathbf{k}_{\perp}}{2(2\pi)^3} |\Psi_{h_q, h_{\bar{q}}}^{(1)L, (T)}(x, \mathbf{k}_{\perp}^2)|^2 = 1. \quad (20)$$

Our spin improved holographic wave functions differ from the ‘‘boosted’’ wave functions in the quark model which are obtained by boosting the nonrelativistic Schrödinger wave function in the rest frame of mesons to the light-front. Our holographic wave functions are directly formulated in the light-front and are frame-independent, avoiding the ambiguities associated with a boosting prescription. These two wave functions differ by a factor of $1/\sqrt{x(1-x)}$ which is mainly responsible for better results in the present case. In our wave function, the AdS/QCD scale parameter κ is extracted from the mass spectroscopic data, which fixes the width of the holographic Gaussian. While in boosted wave function, width of the boosted Gaussian is a free parameter and has to be fixed by some constraint on the wave function. The TMDs and PDFs for light vector mesons have been successfully studied with LFHM. We have extended the model for heavy vector mesons J/ψ and Υ as very less work is available for the theoretical predictions of TMDs and PDFs for these heavy vector mesons.

C. Light-front quark model

LFQM focuses on the valence quarks which are the primary constituents responsible for the overall structure and properties of hadrons [51–58]. The LFHM is basically an extension of LFQM. The momentum wave function from Brodsky-Huang-Lepage (BHL) prescription, in the LFQM, is given as [79–82]

$$\psi^{(2)}(x, \mathbf{k}_{\perp}^2) = \mathcal{N} \exp \left[-\frac{1}{8\beta^2} \left(\frac{\mathbf{k}_{\perp}^2 + m_q^2}{x} + \frac{\mathbf{k}_{\perp}^2 + m_{\bar{q}}^2}{1-x} \right) \right]. \quad (21)$$

Here β is a model parameter and its value is 0.699 GeV for J/ψ and 1.376 GeV for Υ meson [83]. Since we are dealing with the $c\bar{c}$ and $b\bar{b}$ systems here, the quark masses follow the relation $m_q = m_{\bar{q}}$. Therefore, Eq. (21) can now be expressed as

$$\psi^{(2)}(x, \mathbf{k}_{\perp}^2) = \mathcal{N} \exp \left[-\frac{\mathbf{k}_{\perp}^2 + m_q^2}{8\beta^2 x(1-x)} \right]. \quad (22)$$

By taking into account the spin part on the spin projection of J/ψ and Υ [79,80], Eq. (22) becomes

$$\Psi_{h_q, h_{\bar{q}}}^{(2)\Lambda}(x, \mathbf{k}_{\perp}^2) = \chi_{h_q, h_{\bar{q}}}^{(2)\Lambda}(x, \mathbf{k}_{\perp}) \psi^{(2)}(x, \mathbf{k}_{\perp}^2), \quad (23)$$

with the normalization

$$\sum_{h_q, h_{\bar{q}}} \chi_{h_q, h_{\bar{q}}}^{(2)\Lambda*}(x, \mathbf{k}_{\perp}) \chi_{h_q, h_{\bar{q}}}^{(2)\Lambda}(x, \mathbf{k}_{\perp}) = 1. \quad (24)$$

The spin part of Eq. (23) has already been calculated for the longitudinal (L) and transverse (T) spin projections from instant form to the front form through Melosh-Wigner method [80]. For the longitudinal spin projection $\Lambda = L$, $\chi_{h_q, h_{\bar{q}}}^{(2)\Lambda}$ is given as

$$\begin{aligned} \chi_{+,+}^{(2)L}(x, \mathbf{k}_{\perp}) &= \frac{(1-2x)M_{\alpha}k_L}{(M_{\alpha} + 2m_q)\sqrt{2(\mathbf{k}_{\perp}^2 + m_q^2)}}, \\ \chi_{+,-}^{(2)L}(x, \mathbf{k}_{\perp}) &= \frac{m_q(M_{\alpha} + 2m_q) + 2\mathbf{k}_{\perp}^2}{(M_{\alpha} + 2m_q)\sqrt{2(\mathbf{k}_{\perp}^2 + m_q^2)}}, \\ \chi_{-,+}^{(2)L}(x, \mathbf{k}_{\perp}) &= \frac{m_q(M_{\alpha} + 2m_q) + 2\mathbf{k}_{\perp}^2}{(M_{\alpha} + 2m_q)\sqrt{2(\mathbf{k}_{\perp}^2 + m_q^2)}}, \\ \chi_{-,-}^{(2)L}(x, \mathbf{k}_{\perp}) &= -\frac{(1-2x)M_{\alpha}k_R}{(M_{\alpha} + 2m_q)\sqrt{2(\mathbf{k}_{\perp}^2 + m_q^2)}}. \end{aligned}$$

For the transverse spin projection $\Lambda = T(+)$, we have

$$\begin{aligned} \chi_{+,+}^{(2)T(+)}(x, \mathbf{k}_{\perp}) &= \frac{m_q(M_{\alpha} + 2m) + \mathbf{k}_{\perp}^2}{(M_{\alpha} + 2m_q)\sqrt{\mathbf{k}_{\perp}^2 + m_q^2}}, \\ \chi_{+,-}^{(2)T(+)}(x, \mathbf{k}_{\perp}) &= \frac{(xM_{\alpha} + m_q)k_R}{(M_{\alpha} + 2m_q)\sqrt{\mathbf{k}_{\perp}^2 + m_q^2}}, \\ \chi_{-,+}^{(2)T(+)}(x, \mathbf{k}_{\perp}) &= -\frac{((1-x)M_{\alpha} + m_q)k_R}{(M_{\alpha} + 2m_q)\sqrt{\mathbf{k}_{\perp}^2 + m_q^2}}, \\ \chi_{-,-}^{(2)T(+)}(x, \mathbf{k}_{\perp}) &= -\frac{k_R^2}{(M_{\alpha} + 2m_q)\sqrt{\mathbf{k}_{\perp}^2 + m_q^2}}, \end{aligned}$$

and for $\Lambda = T(-)$, we have

$$\chi_{+,+}^{(2)T(-)}(x, \mathbf{k}_\perp) = -\frac{k_L^2}{(M_\alpha + 2m_q)\sqrt{\mathbf{k}_\perp^2 + m_q^2}},$$

$$\chi_{+,-}^{(2)T(-)}(x, \mathbf{k}_\perp) = \frac{((1-x)M_\alpha + m_q)k_L}{(M_\alpha + 2m_q)\sqrt{\mathbf{k}_\perp^2 + m_q^2}},$$

$$\chi_{-,+}^{(2)T(-)}(x, \mathbf{k}_\perp) = -\frac{(xM_\alpha + m_q)k_L}{(M_\alpha + 2m_q)\sqrt{\mathbf{k}_\perp^2 + m_q^2}},$$

$$\chi_{-,-}^{(2)T(-)}(x, \mathbf{k}_\perp) = \frac{m_q(M_\alpha + 2m_q) + \mathbf{k}_\perp^2}{(M_\alpha + 2m_q)\sqrt{\mathbf{k}_\perp^2 + m_q^2}},$$

with

$$M_\alpha = \sqrt{\frac{\mathbf{k}_\perp^2 + m_q^2}{x(1-x)}}.$$

Now the LFWFs of Eq. (23) can be written explicitly for longitudinal projection $\Lambda = L$ as

$$\Psi_{+,+}^{(2)L}(x, \mathbf{k}_\perp^2) = \frac{(1-2x)M_\alpha k_L}{\sqrt{2}\omega} \psi^{(2)}(x, \mathbf{k}_\perp^2), \quad (25)$$

$$\Psi_{+,-}^{(2)L}(x, \mathbf{k}_\perp^2) = \frac{m_q(M_\alpha + 2m_q) + 2\mathbf{k}_\perp^2}{\sqrt{2}\omega} \psi^{(2)}(x, \mathbf{k}_\perp^2), \quad (26)$$

$$\Psi_{-,+}^{(2)L}(x, \mathbf{k}_\perp^2) = \frac{m_q(M_\alpha + 2m_q) + 2\mathbf{k}_\perp^2}{\sqrt{2}\omega} \psi^{(2)}(x, \mathbf{k}_\perp^2), \quad (27)$$

$$\Psi_{-,-}^{(2)L}(x, \mathbf{k}_\perp^2) = \frac{(1-2x)M_\alpha k_R}{\sqrt{2}\omega} \psi^{(2)}(x, \mathbf{k}_\perp^2). \quad (28)$$

For transverse projection $\Lambda = T(+)$, the LFWFs are

$$\Psi_{+,+}^{(2)T(+)}(x, \mathbf{k}_\perp^2) = \frac{m_q(M_\alpha + 2m) + \mathbf{k}_\perp^2}{\omega} \psi^{(2)}(x, \mathbf{k}_\perp^2), \quad (29)$$

$$\Psi_{+,+}^{(2)T(+)}(x, \mathbf{k}_\perp^2) = \frac{(xM_\alpha + m_q)k_R}{\omega} \psi^{(2)}(x, \mathbf{k}_\perp^2), \quad (30)$$

$$\Psi_{-,+}^{(2)T(+)}(x, \mathbf{k}_\perp^2) = -\frac{((1-x)M_\alpha + m_q)k_R}{\omega} \psi^{(2)}(x, \mathbf{k}_\perp^2), \quad (31)$$

$$\Psi_{-,-}^{(2)T(+)}(x, \mathbf{k}_\perp^2) = -\frac{k_R^2}{\omega} \psi^{(2)}(x, \mathbf{k}_\perp^2), \quad (32)$$

and for $\Lambda = T(-)$, the LFWFs are

$$\Psi_{+,+}^{(2)T(-)}(x, \mathbf{k}_\perp^2) = -\frac{k_L^2}{\omega} \psi^{(2)}(x, \mathbf{k}_\perp^2), \quad (33)$$

$$\Psi_{+,+}^{(2)T(-)}(x, \mathbf{k}_\perp^2) = \frac{((1-x)M_\alpha + m_q)k_L}{\omega} \psi^{(2)}(x, \mathbf{k}_\perp^2), \quad (34)$$

$$\Psi_{-,+}^{(2)T(-)}(x, \mathbf{k}_\perp^2) = -\frac{(xM_\alpha + m_q)k_L}{\omega} \psi^{(2)}(x, \mathbf{k}_\perp^2), \quad (35)$$

$$\Psi_{-,-}^{(2)T(-)}(x, \mathbf{k}_\perp^2) = \frac{m_q(M_\alpha + 2m_q) + \mathbf{k}_\perp^2}{\omega} \psi^{(2)}(x, \mathbf{k}_\perp^2). \quad (36)$$

We have

$$\omega = (M_\alpha + 2m_q)\sqrt{\mathbf{k}_\perp^2 + m_q^2}.$$

LFQM provides very reasonable results in the lower Q^2 region. The LFQM wave functions have been used for the study of $B_i(\frac{1}{2}^+) \rightarrow B_f(\frac{3}{2}^+)$ transitions [84], $\Xi_{cc} \rightarrow \Xi_c$ weak decay [85], $V' \rightarrow V''$ transition [86], $(\pi^0, \eta, \eta') \rightarrow \gamma^* \gamma^*$ transitions [87] etc. LFQM has also been used for calculating the form factors (FFs), distribution amplitudes (DAs) etc. [83,88–90].

D. Overlap form of the LFWFs

The overlap form of the LFWFs in terms of the LF helicity amplitudes with quark and antiquark helicities along with their polarizations for the heavy vector mesons for both the models can be expressed as [42,43]

$$A_{h'_q \Lambda', h_q \Lambda}(x, \mathbf{k}_\perp^2) = \frac{1}{(2\pi)^3} \sum_{h_{\bar{q}}} \Psi_{h'_q, h_{\bar{q}}}^{(n)\Lambda'^*}(x, \mathbf{k}_\perp^2) \Psi_{h_q, h_{\bar{q}}}^{(n)\Lambda}(x, \mathbf{k}_\perp^2). \quad (37)$$

Here $n = 1$ and 2 for the LFHM and LFQM respectively. The explicit overlap form for all the T -even TMDs in terms of helicity amplitudes for both the models is given by [42]

$$f_1(x, \mathbf{k}_\perp^2) = \frac{1}{6}(A_{+,+,+} + A_{-,-,-} + A_{+,+,+} + A_{-,-,-} + A_{+,-,+} + A_{-,-,-}), \quad (38)$$

$$g_{1L}(x, \mathbf{k}_\perp^2) = \frac{1}{4}(A_{+,+,+} - A_{-,-,-} - A_{+,-,+} + A_{-,-,-}), \quad (39)$$

$$g_{1T}(x, \mathbf{k}_\perp^2) = \frac{M_\alpha}{4\sqrt{2}\mathbf{k}_\perp^2} (k_R(A_{+,+,+} - A_{-,-,-} + A_{+,+,-} - A_{-,-,-}) + k_L(A_{+,+,+} - A_{-,-,-} + A_{+,-,+} - A_{-,-,-})), \quad (40)$$

$$h_1(x, \mathbf{k}_\perp^2) = \frac{1}{4\sqrt{2}}(A_{++,-0} + A_{-0,++} + A_{+0,-} + A_{--,+0}), \quad (41)$$

$$h_{1L}^\perp(x, \mathbf{k}_\perp^2) = \frac{M_\alpha}{4\mathbf{k}_\perp^2}(k_R(A_{-+,++} - A_{--,+-}) + k_L(A_{++,-} - A_{+,-})), \quad (42)$$

$$h_{1T}^\perp(x, \mathbf{k}_\perp^2) = \frac{M_\alpha^2}{2\sqrt{2}\mathbf{k}_\perp^4}(k_R^2(A_{-+,+0} + A_{-0,+}) + k_L^2(A_{+0,-} + A_{+,-,0})), \quad (43)$$

$$f_{1LL}(x, \mathbf{k}_\perp^2) = \frac{1}{2}A_{+0,+0} + A_{-0,-0} - \frac{1}{4}(A_{++,+} + A_{-,-,+} + A_{+,-,+} + A_{--,-}), \quad (44)$$

$$f_{1LT}(x, \mathbf{k}_\perp^2) = \frac{M_\alpha}{4\sqrt{2}\mathbf{k}_\perp^2}(k_R(A_{++,+0} + A_{-+,-0} - A_{+0,+} - A_{-0,-}) \\ + k_L(A_{+0,+} + A_{-0,-} - A_{+,-,+} - A_{--,-})), \quad (45)$$

$$f_{1TT}(x, \mathbf{k}_\perp^2) = \frac{M_\alpha^2}{4\sqrt{2}\mathbf{k}_\perp^4}(k_R^2(A_{++,+} + A_{-+,-}) + k_L^2(A_{+,-,+} + A_{--,-})). \quad (46)$$

Substituting Eqs. (25)–(36) in the above LF helicity amplitude equations, through Eq. (37) for $n = 2$, the T -even TMDs for LFQM can be computed and are expressed as

$$f_1(x, \mathbf{k}_\perp^2) = \frac{1}{3(2\pi)^3} \left(\frac{1}{2}(3(m_q(M_\alpha + 2m_q))^2 + (1 - 2x)^2 M_\alpha^2 \mathbf{k}_\perp^2) + 4\mathbf{k}_\perp^2(m_q(M_\alpha + 2m_q) + \mathbf{k}_\perp^2) \right. \\ \left. + \mathbf{k}_\perp^2(2m_q(M_\alpha + m_q) + M_\alpha^2(1 - 2x + 2x^2)) \right) \frac{|\psi^{(2)}(x, \mathbf{k}_\perp^2)|^2}{\omega^2}, \quad (47)$$

$$g_{1L}(x, \mathbf{k}_\perp^2) = \frac{1}{2(2\pi)^3} (m_q(M_\alpha + 2m_q)(m_q(M_\alpha + 2m_q) + 2\mathbf{k}_\perp^2) - M_\alpha(M_\alpha + 2m_q)(1 - 2x)) \frac{|\psi^{(2)}(x, \mathbf{k}_\perp^2)|^2}{\omega^2}, \quad (48)$$

$$g_{1T}(x, \mathbf{k}_\perp^2) = \frac{M_\alpha}{2(2\pi)^3} (M_\alpha + 2m_q)(m_q M_\alpha(1 - 2x) + (2\mathbf{k}_\perp^2 + m_q(M_\alpha + 2m_q))) \times \frac{|\psi^{(2)}(x, \mathbf{k}_\perp^2)|^2}{\omega^2}, \quad (49)$$

$$h_1(x, \mathbf{k}_\perp^2) = \frac{1}{2(2\pi)^3} ((m_q(M_\alpha + 2m_q) + 2\mathbf{k}_\perp^2)(m_q(M_\alpha + 2m_q) + \mathbf{k}_\perp^2) \\ - \mathcal{M}_\alpha(xM_\alpha + m_q)(1 - 2x)\mathbf{k}_\perp^2) \frac{|\psi^{(2)}(x, \mathbf{k}_\perp^2)|^2}{\omega^2}, \quad (50)$$

$$h_{1L}^\perp(x, \mathbf{k}_\perp^2) = -\frac{M_\alpha}{(2\pi)^3} (M_\alpha + 2m_q)(m_q((1 - x)M_\alpha + m_q) + \mathbf{k}_\perp^2) \frac{|\psi^{(2)}(x, \mathbf{k}_\perp^2)|^2}{\omega^2}, \quad (51)$$

$$h_{1T}^\perp(x, \mathbf{k}_\perp^2) = -\frac{M_\alpha^2}{(2\pi)^3} (M_\alpha(m_q + (1 - x)M_\alpha)(1 - 2x) + (2\mathbf{k}_\perp^2 + m_q(M_\alpha + 2m_q))) \times \frac{|\psi^{(2)}(x, \mathbf{k}_\perp^2)|^2}{\omega^2}, \quad (52)$$

$$f_{1LL}(x, \mathbf{k}_\perp^2) = 0, \quad (53)$$

$$f_{1LT}(x, \mathbf{k}_\perp^2) = 0, \quad (54)$$

$$f_{1TT}(x, \mathbf{k}_\perp^2) = 0. \quad (55)$$

Similarly, substituting Eqs. (18) and (19) in Eqs. (38)–(46) through Eq. (37) for $n = 1$, the T -even TMDs in LFHM can be derived and are expressed as

$$f_1(x, \mathbf{k}_\perp^2) = \frac{1}{3(2\pi)^3} \left(\mathcal{N}_L^2 (M_\alpha^2 x(1-x) + m_q^2 + \mathbf{k}_\perp^2)^2 \frac{|\psi^{(1)}(x, \mathbf{k}_\perp^2)|^2}{x^2(1-x)^2} + \mathcal{N}_T^2 (m_q^2 + \mathbf{k}_\perp^2 (2x^2 - 2x + 1)) \frac{|\psi^{(1)}(x, \mathbf{k}_\perp^2)|^2}{x^2(1-x)^2} \right), \quad (56)$$

$$g_{1L}(x, \mathbf{k}_\perp^2) = \frac{\mathcal{N}_T^2}{2(2\pi)^3} (m_q^2 + \mathbf{k}_\perp^2 (2x - 1)) \frac{|\psi^{(1)}(x, \mathbf{k}_\perp^2)|^2}{x^2(1-x)^2}, \quad (57)$$

$$g_{1T}(x, \mathbf{k}_\perp^2) = \mathcal{N}_L \mathcal{N}_T \frac{M_\alpha}{\sqrt{2}(2\pi)^3} (M_\alpha^2 x(1-x) + m_q^2 + \mathbf{k}_\perp^2) \frac{|\psi^{(1)}(x, \mathbf{k}_\perp^2)|^2}{x^2(1-x)^2}, \quad (58)$$

$$h_1(x, \mathbf{k}_\perp^2) = \mathcal{N}_L \mathcal{N}_T \frac{m_q}{\sqrt{2}(2\pi)^3} (M_\alpha^2 x(1-x) + m_q^2 + \mathbf{k}_\perp^2) \frac{|\psi^{(1)}(x, \mathbf{k}_\perp^2)|^2}{x^2(1-x)^2}, \quad (59)$$

$$h_{1L}^\perp(x, \mathbf{k}_\perp^2) = -\mathcal{N}_T^2 \frac{m_q M_\alpha}{(2\pi)^3} \frac{|\psi^{(1)}(x, \mathbf{k}_\perp^2)|^2}{x^2(1-x)}, \quad (60)$$

$$h_{1T}^\perp(x, \mathbf{k}_\perp^2) = 0, \quad (61)$$

$$f_{1LL}(x, \mathbf{k}_\perp^2) = \frac{1}{(2\pi)^3} \left(\mathcal{N}_L^2 (M_\alpha^2 x(1-x) + m_q^2 + \mathbf{k}_\perp^2)^2 \frac{|\psi^{(1)}(x, \mathbf{k}_\perp^2)|^2}{x^2(1-x)^2} - \mathcal{N}_T^2 (m_q^2 + \mathbf{k}_\perp^2 (2x^2 - 2x + 1)) \frac{|\psi^{(1)}(x, \mathbf{k}_\perp^2)|^2}{2x^2(1-x)^2} \right), \quad (62)$$

$$f_{1LT}(x, \mathbf{k}_\perp^2) = \mathcal{N}_L \mathcal{N}_T \frac{M_\alpha}{\sqrt{2}(2\pi)^3} (2x - 1) (M_\alpha^2 x(1-x) + m_q^2 + \mathbf{k}_\perp^2) \frac{|\psi^{(1)}(x, \mathbf{k}_\perp^2)|^2}{x^2(1-x)^2}, \quad (63)$$

$$f_{1TT}(x, \mathbf{k}_\perp^2) = \mathcal{N}_T^2 \frac{M_\alpha^2}{(2\pi)^3} \frac{|\psi^{(1)}(x, \mathbf{k}_\perp^2)|^2}{x(1-x)}. \quad (64)$$

Equations (47)–(55) are the T -even TMDs in the LFQM and Eqs. (56)–(64) are in the LFHM. Angular momentum along z -axis is conserved for all the TMDs. There is zero orbital angular momentum (OAM) transfer between initial and final state of the hadron for f_1 , g_{1L} , h_{1L}^\perp and f_{1LL} TMDs. Equations (57), (60), and (64) are the overlapping LFWFs for $\Lambda = \pm 1$, therefore, these TMDs have the factor of \mathcal{N}_T^2 . Equations (58) and (59) are (63) are a consequence of $\Lambda = 0$ to $\Lambda = \pm 1$ overlapping, therefore, they have a $\mathcal{N}_L \mathcal{N}_T$ factor. Equations (56) and (62) do not have a common factor. In the LFQM, f_{1LL} , f_{1LT} and f_{1TT} come out to be zero whereas in the LFHM, h_{1T}^\perp TMD is zero. Since the higher Fock-states are suppressed in case of heavy vector mesons [42], we have considered the lower Fock-states only for both the models which provides good results.

E. Numerical results

For the numerical predictions of J/ψ and Υ meson TMDs in the LFHM, we have used the universal AdS/QCD scale $\kappa = 0.894$ GeV with quark mass $m_c = 1.5$ GeV for the case of J/ψ -meson [70] and $\kappa = 1.49$ GeV with quark mass $m_b = 4.63$ GeV for the case of Υ -meson [71]. Similarly, in the LFQM, we have used $\beta = 0.699$ GeV with quark mass $m_c = 1.68$ GeV for the case of J/ψ -meson and $\beta = 1.376$ GeV with quark mass $m_b = 5.10$ GeV for the case of Υ -meson [83]. In Figs. 1–5, we illustrate the J/ψ and Υ meson TMDs in the LFHM results at model scale $\mu_{\text{LFHM}}^2 = 0.20$ GeV² and compare them with the LFQM at model scale $\mu_{\text{LFQM}}^2 = 0.19$ GeV². The model scale has been taken from the Ref. [43]. On the left side of the Figs. 1–6, we have presented the 2D J/ψ meson TMD's comparison in both LFHM and LFQM.

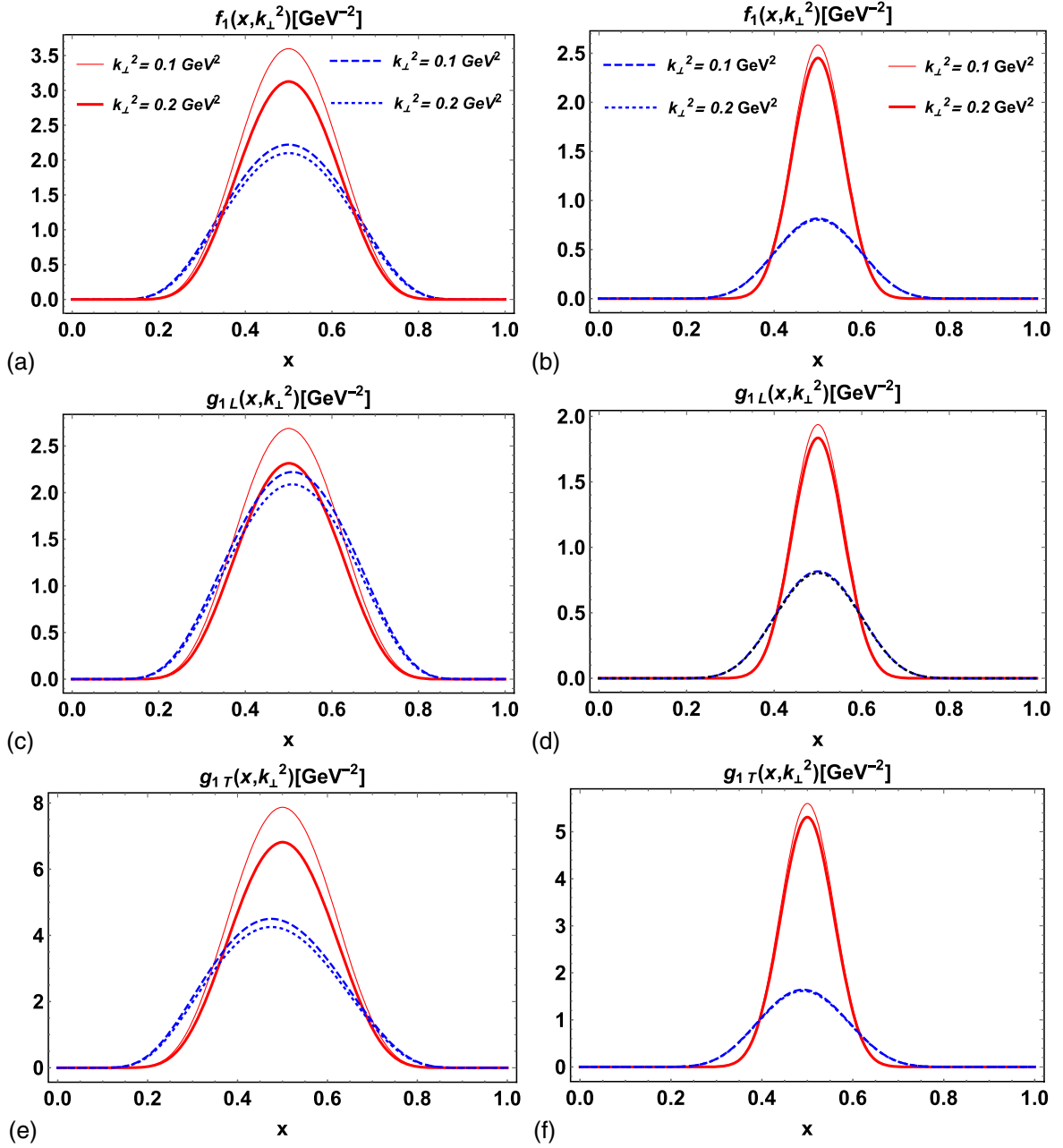


FIG. 1. (a,b) $f_1(x, \mathbf{k}_\perp^2)$, (c,d) $g_{1L}(x, \mathbf{k}_\perp^2)$, and (e,f) $g_{1T}(x, \mathbf{k}_\perp^2)$ TMDs are plotted with respect to x at different values of \mathbf{k}_\perp^2 , i.e., $\mathbf{k}_\perp^2 = 0.1 \text{ GeV}^2$ and $\mathbf{k}_\perp^2 = 0.2 \text{ GeV}^2$. The solid red thick and thin curves represents the TMDs in LFHM, while blue dot and dashed curves are for LFQM. The TMDs comparison of J/ψ and Υ meson in the LFHM and LFQM at the model scale $\mu_{\text{LFHM}}^2 = 0.20 \text{ GeV}^2$ and $\mu_{\text{LFQM}}^2 = 0.19 \text{ GeV}^2$ in the left and right panels, respectively.

While on the right side, Υ meson TMD's comparison with respect to x and \mathbf{k}_\perp^2 has been presented for both the models. In all the figures, we have used red (thick, thin) and blue (dashed, dotted) lines for LFHM and LFQM respectively.

In Fig. 1, we have presented the unpolarized quark TMD, $f_1(x, \mathbf{k}_\perp^2)$ as well as the longitudinally polarized quark TMDs: $g_{1L}(x, \mathbf{k}_\perp^2)$ and $g_{1T}(x, \mathbf{k}_\perp^2)$ for both the particles in both the models. All the TMDs in Fig. 1 are functions of x at different fixed values of \mathbf{k}_\perp^2 . The qualitative behavior of

$f_1(x, \mathbf{k}_\perp^2)$, $g_{1L}(x, \mathbf{k}_\perp^2)$ and $g_{1T}(x, \mathbf{k}_\perp^2)$ in the LFHM are consistent with those of the LFQM. This is true for both the J/ψ and Υ mesons. Even though the behavior of all the plots look similar, however they have different peak values. In the case of LFHM, the particles have higher peak values compared to the LFQM. At $\mathbf{k}_\perp^2 = 0.2 \text{ GeV}^2$, both J/ψ and Υ have almost same peak values for $g_{1L}(x, \mathbf{k}_\perp^2)$ TMD in Fig. 1(c). The $g_{1T}(x, \mathbf{k}_\perp^2)$ TMD has higher peak value than the other TMDs and carry highest transverse momentum in

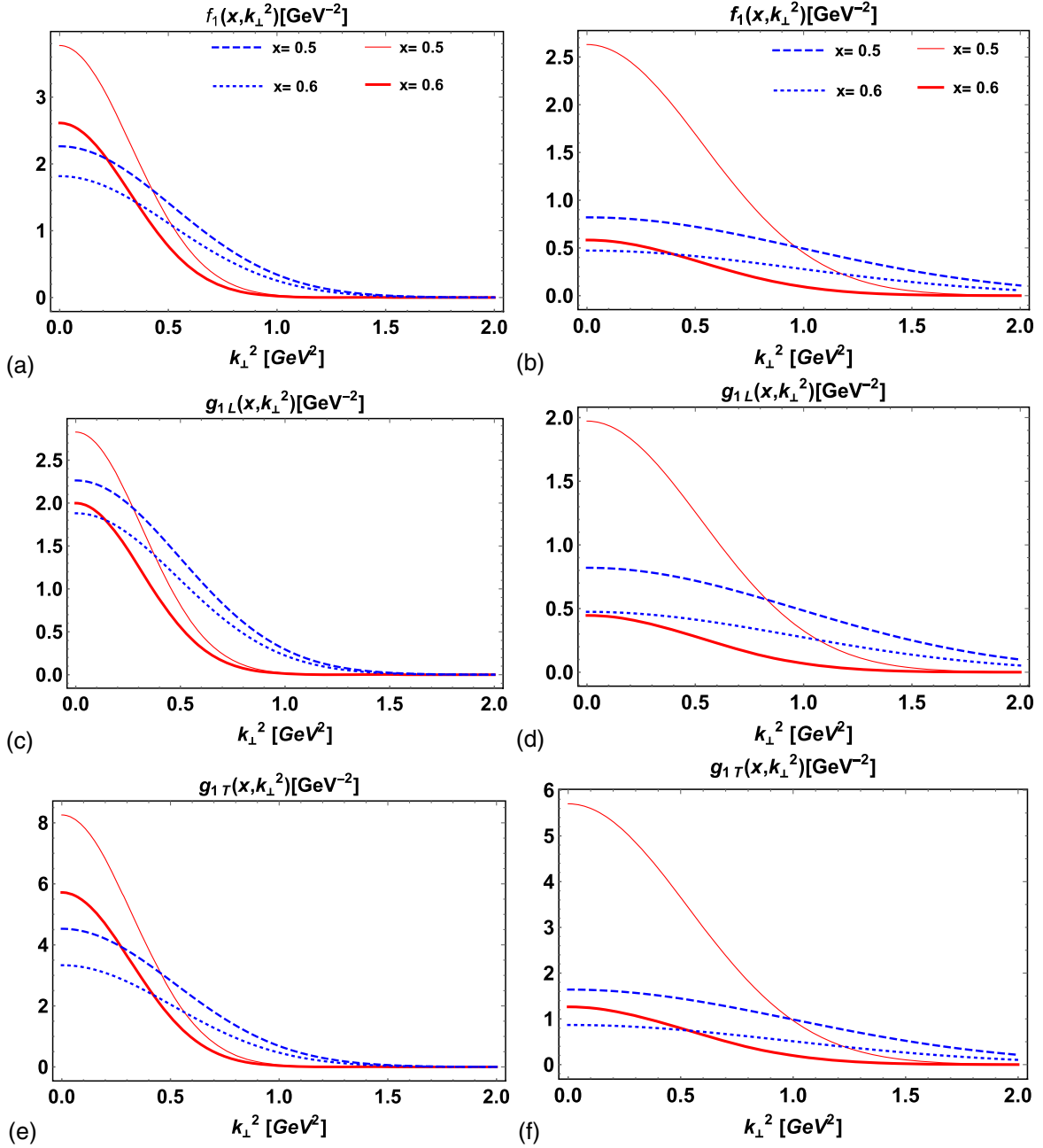


FIG. 2. (a,b) $f_1(x, \mathbf{k}_\perp^2)$, (c,d) $g_{1L}(x, \mathbf{k}_\perp^2)$, and (e,f) $g_{1T}(x, \mathbf{k}_\perp^2)$ TMDs are plotted with respect to \mathbf{k}_\perp^2 at different values of x i.e., $x = 0.5$ and $x = 0.6$. The solid red thick and thin curves represents the TMDs in LFHM, while blue dot and dashed curves are for LFQM. The TMDs comparison of J/ψ and Υ meson in the LFHM and LFQM at the model scale $\mu_{\text{LFHM}}^2 = 0.20 \text{ GeV}^2$ and $\mu_{\text{LFQM}}^2 = 0.19 \text{ GeV}^2$ in the left and right panels, respectively.

LFHM. While in the case of LFQM, $h_{1T}(x, \mathbf{k}_\perp^2)$ has higher transverse momentum for both the particles. As we move toward higher quark masses values, the quark TMDs become narrower with x and broader with \mathbf{k}_\perp^2 . As the Υ meson is less relativistic than J/ψ meson, the TMDs become narrower for Υ and broader for J/ψ . All the quark TMDs are centered at $x = 0.5$ and low \mathbf{k}_\perp^2 . In Fig. 2, we demonstrate $f_1(x, \mathbf{k}_\perp^2)$, $g_{1L}(x, \mathbf{k}_\perp^2)$, and $g_{1T}(x, \mathbf{k}_\perp^2)$ TMDs

as a function of \mathbf{k}_\perp^2 at different fixed values of x in LFHM (left panel) and LFQM (right panel). These TMDs decrease monotonically with respect to \mathbf{k}_\perp^2 indicating heavy quark and anti-quark have low relative momentum. All the figures have a similar trend in both the models. In Fig. 2, the J/ψ meson TMDs are found to be zero for $\mathbf{k}_\perp^2 \geq 2 \text{ GeV}^2$ for both the models. The heavy Υ carries higher transverse momentum than the J/ψ -meson.

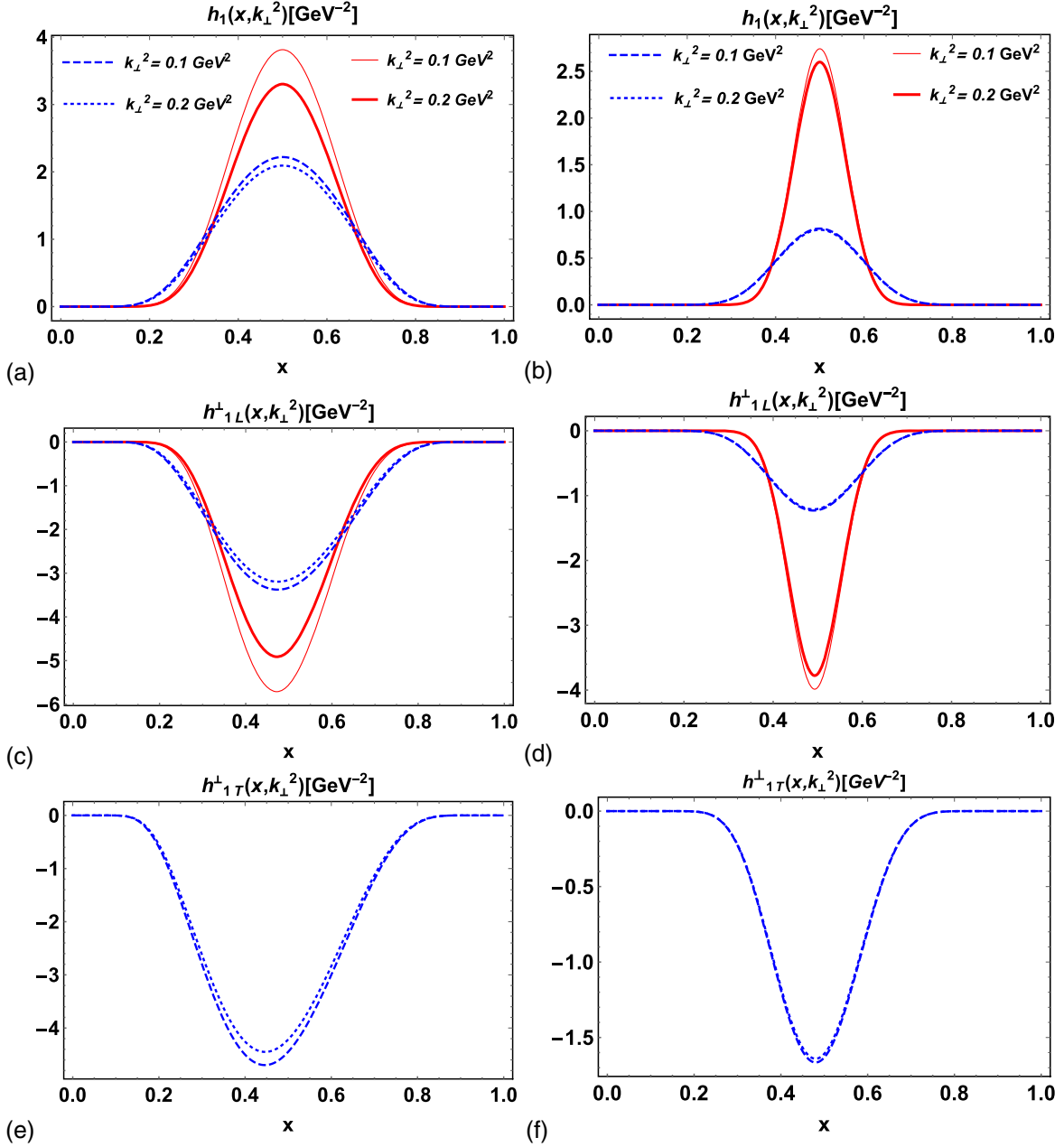


FIG. 3. (a,b) $h_1(x, \mathbf{k}_\perp^2)$, (c,d) $h_{1L}^\perp(x, \mathbf{k}_\perp^2)$, and (e,f) $h_{1T}^\perp(x, \mathbf{k}_\perp^2)$ TMDs are plotted with respect to x at different values of \mathbf{k}_\perp^2 , i.e., $\mathbf{k}_\perp^2 = 0.1 \text{ GeV}^2$ and $\mathbf{k}_\perp^2 = 0.2 \text{ GeV}^2$. The solid red thick and thin curves represents the TMDs in LFHM, while blue dot and dashed curves are for LFQM. The TMDs comparison of J/Ψ and Υ meson in the LFHM and LFQM at the model scale $\mu_{\text{LFHM}}^2 = 0.20 \text{ GeV}^2$ and $\mu_{\text{LFQM}}^2 = 0.19 \text{ GeV}^2$ in the left and right panels, respectively.

The TMDs $f_1(x, \mathbf{k}_\perp^2)$, $g_{1T}(x, \mathbf{k}_\perp^2)$ and $g_{1L}(x, \mathbf{k}_\perp^2)$ describe the momentum distributions of the unpolarized quark in the unpolarized meson, the longitudinally polarized quark in the transversely polarized meson and the longitudinally polarized quark in the longitudinally polarized meson respectively. The S-wave is more dominant in the case of heavy vector meson TMDs as compared to the P-wave and D-wave. Due to this dominance, all the TMDs in Fig. 1 follow symmetry under $x \leftrightarrow (1-x)$ in the LFHM as well as in the LFQM.

In Figs. 3 and 4, we have discussed the transversely polarized TMDs, $h_1(x, \mathbf{k}_\perp^2)$, $h_{1L}^\perp(x, \mathbf{k}_\perp^2)$ and $h_{1T}^\perp(x, \mathbf{k}_\perp^2)$ with respect to x and \mathbf{k}_\perp^2 . In the LFHM, $h_{1T}^\perp(x, \mathbf{k}_\perp^2)$ TMD is zero [43,46], therefore the results have been presented only for the case of LFQM in Figs. 3(e) and 4(e). The TMDs $h_1(x, \mathbf{k}_\perp^2)$ and $h_{1L}^\perp(x, \mathbf{k}_\perp^2)$ describe the momentum distribution of the transversely polarized quark in a transversely and longitudinally polarized meson respectively. $h_{1T}^\perp(x, \mathbf{k}_\perp^2)$ TMD describes the momentum

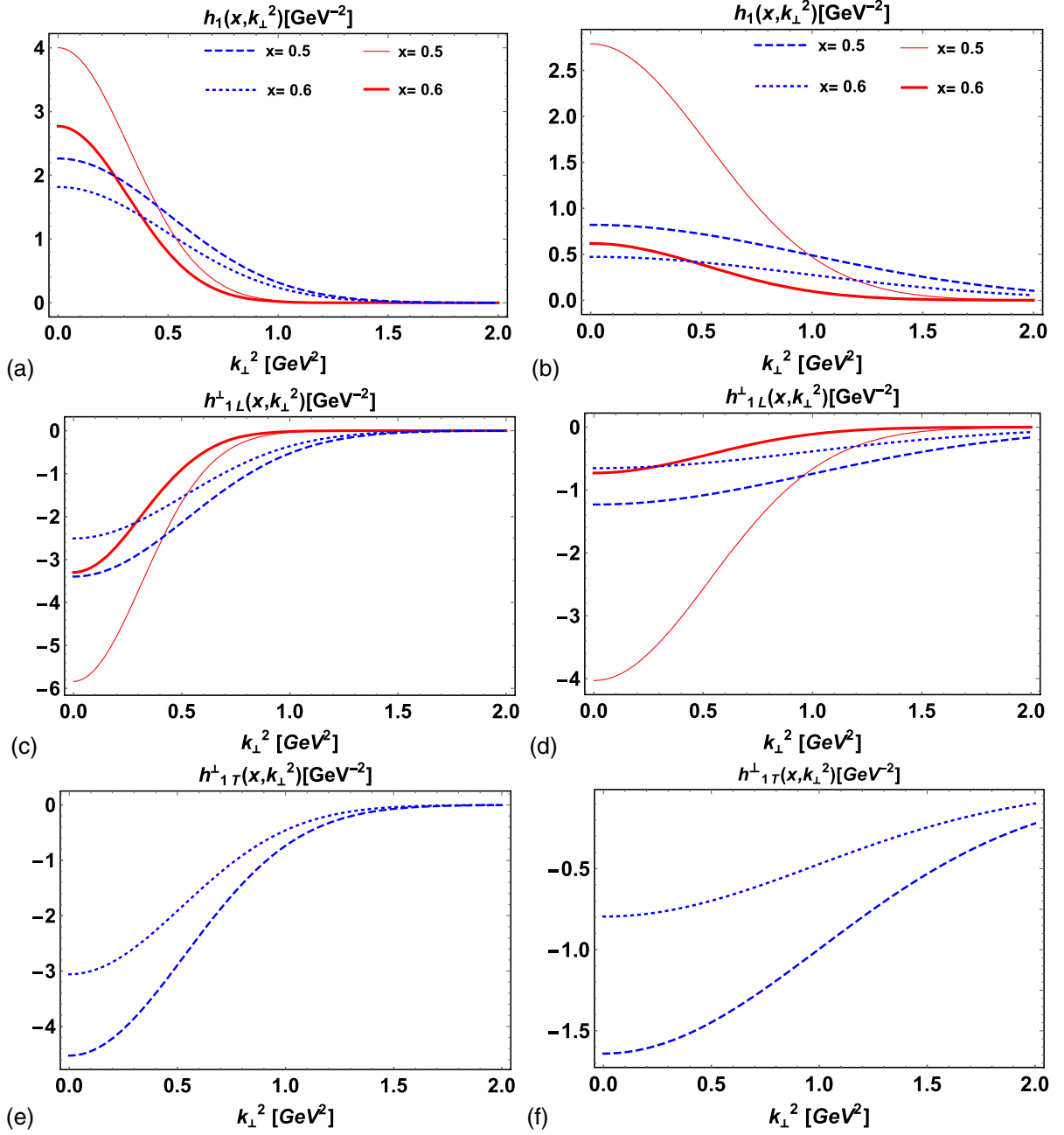


FIG. 4. (a,b) $h_1(x, \mathbf{k}_\perp^2)$, (c,d) $h_{1L}^\perp(x, \mathbf{k}_\perp^2)$, and (e,f) $h_{1T}^\perp(x, \mathbf{k}_\perp^2)$ TMDs are plotted with respect to \mathbf{k}_\perp^2 at different values of x , i.e., $x = 0.5$ and $x = 0.6$. The solid red thick and thin curves represents the TMDs in LFHM, while blue dot and dashed curves are for LFQM. The TMDs comparison of J/Ψ and Υ meson in the LFHM and LFQM at the model scale $\mu_{\text{LFHM}}^2 = 0.20 \text{ GeV}^2$ and $\mu_{\text{LFQM}}^2 = 0.19 \text{ GeV}^2$ in the left and right panels, respectively.

distribution when both the meson and quark are transversely polarized and their polarizations are further perpendicular to each other. The TMD $h_1(x, \mathbf{k}_\perp^2)$ shows symmetry under x . There is one unit of OAM transfer occur for $h_{1L}^\perp(x, \mathbf{k}_\perp^2)$ and $g_{1T}(x, \mathbf{k}_\perp^2)$ TMDs between final and initial state of hadron. In Fig. 3(c), the $h_{1L}^\perp(x, \mathbf{k}_\perp^2)$

TMD shows a negative distribution as is clear from Eq. (60) in LFHM where $h_{1L}^\perp(x, \mathbf{k}_\perp^2)$ TMD has a negative N_T^2 in LFHM and for the LFQM this is due to the negative mass term in Eq. (51). Similarly in Fig. 4, we have plotted $h_1(x, \mathbf{k}_\perp^2)$, $h_{1L}^\perp(x, \mathbf{k}_\perp^2)$, and $h_{1T}^\perp(x, \mathbf{k}_\perp^2)$ as a function of \mathbf{k}_\perp^2 at fixed $x = 0.5, 0.6$ value.

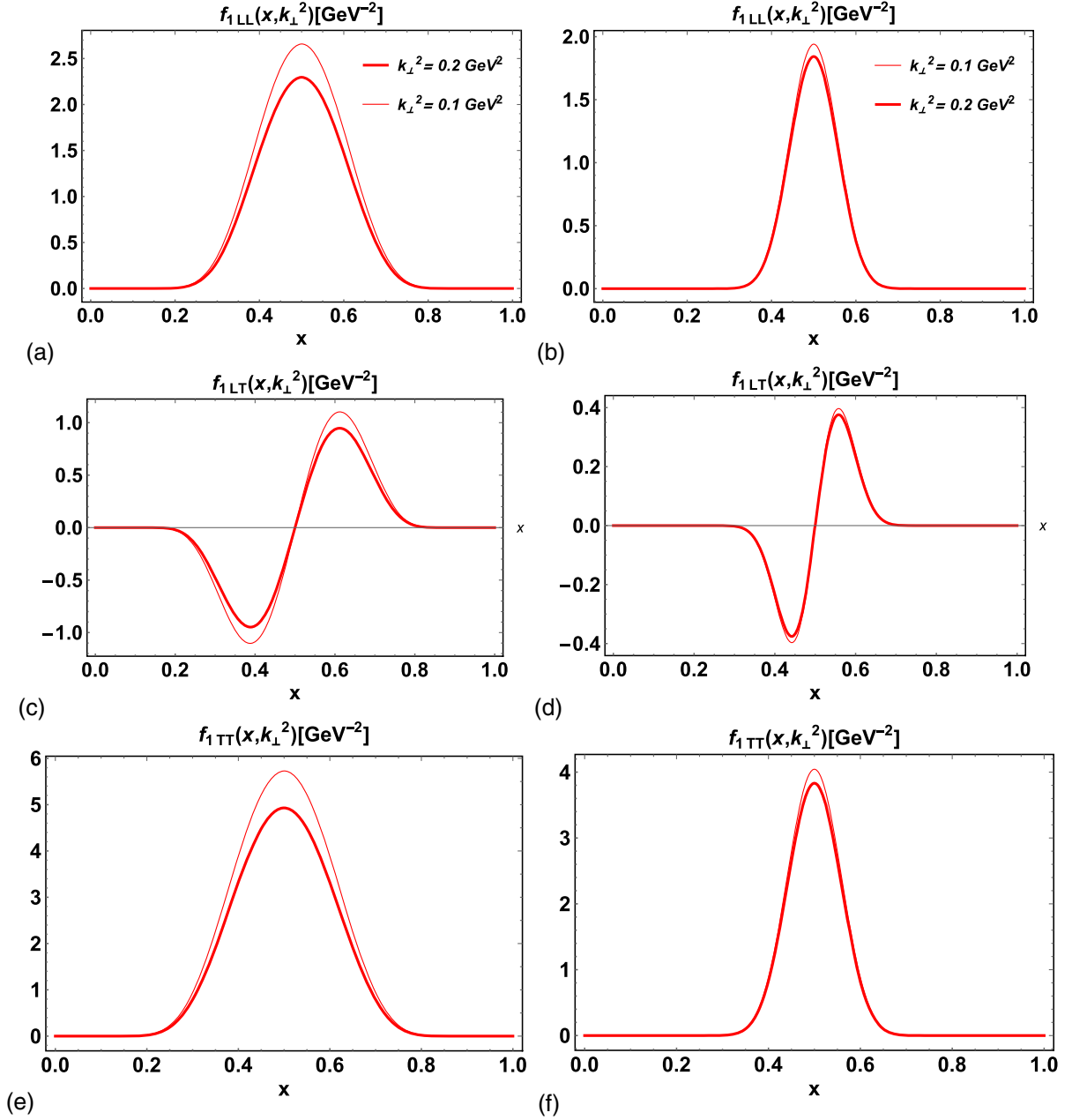


FIG. 5. (a,b) $f_{1LL}(x, \mathbf{k}_{\perp}^2)$, (c,d) $f_{1LT}(x, \mathbf{k}_{\perp}^2)$, and (e,f) $f_{1TT}(x, \mathbf{k}_{\perp}^2)$ TMDs are plotted with respect to x at different values of \mathbf{k}_{\perp}^2 , i.e., $\mathbf{k}_{\perp}^2 = 0.1 \text{ GeV}^2$ (solid thin curves) and $\mathbf{k}_{\perp}^2 = 0.2 \text{ GeV}^2$ (solid thick curves) for LFHM at model scale $\mu_{\text{LFHM}}^2 = 0.20 \text{ GeV}^2$ for J/ψ (left panel) and Υ (right panel) meson, respectively.

Now in Figs. 5 and 6, we have presented the tensor polarized $f_{1LL}(x, \mathbf{k}_{\perp}^2)$, $f_{1LT}(x, \mathbf{k}_{\perp}^2)$, and $f_{1TT}(x, \mathbf{k}_{\perp}^2)$ TMDs as a function of x at fixed \mathbf{k}_{\perp}^2 and as a function of \mathbf{k}_{\perp}^2 at fixed x in LFHM respectively. For the case of LFQM, the tensor polarized quark TMDs are zero because of the different spin structure of the hadron. In Fig. 5(a), $f_{1LL}(x, \mathbf{k}_{\perp}^2)$ shows a symmetry under $x \leftrightarrow (1-x)$. The TMD $f_{1LL}(x, \mathbf{k}_{\perp}^2)$ has a zero OAM from initial to final state of hadron in Eq. (62). For the case of ρ vector meson, the plot of $f_{1LL}(x, \mathbf{k}_{\perp}^2)$ has both positive and negative

distribution but as we move to heavy quark masses, there is only positive distribution as the S-wave contribution increases in heavy quark masses. In Fig. 5, we can clearly see that the $f_{1LT}(x, \mathbf{k}_{\perp}^2)$ vanishes at $x=0.5$, exhibits positive distribution for $x > 0.5$ and negative distribution for $x < 0.5$. The overlap form of $f_{1LT}(x, \mathbf{k}_{\perp}^2)$ quark TMD observed due to the transfer of one unit of OAM from initial to final state of hadron. f_{1LT} is anti-symmetric under the $x \leftrightarrow (1-x)$. An interesting fact about $f_{1LL}(x, \mathbf{k}_{\perp}^2)$ and $f_{1LT}(x, \mathbf{k}_{\perp}^2)$ is that, the J/ψ meson has a higher peak

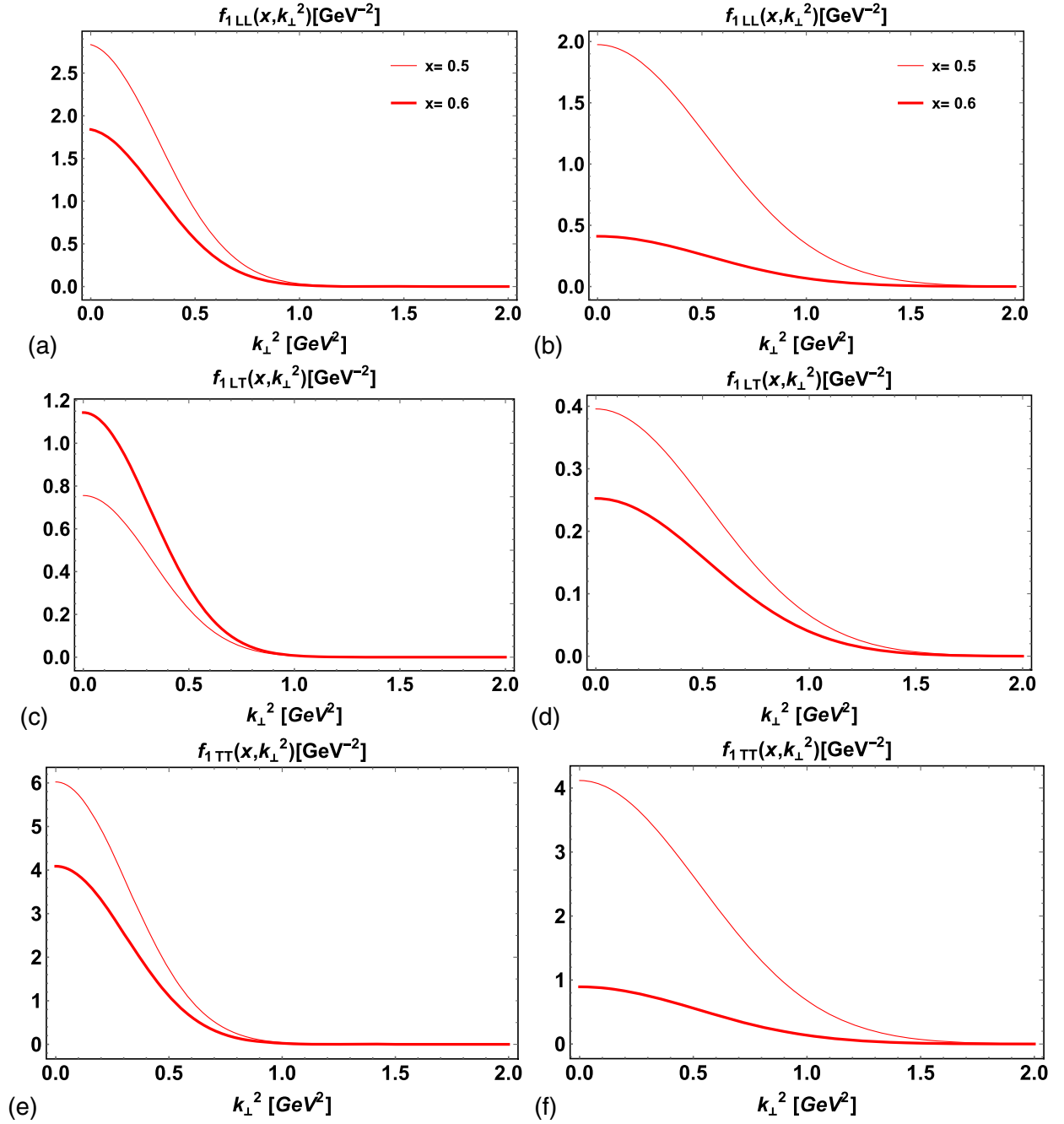


FIG. 6. (a,b) $f_{1LL}(x, \mathbf{k}_\perp^2)$, (c,d) $f_{1LT}(x, \mathbf{k}_\perp^2)$, and (e,f) $f_{1TT}(x, \mathbf{k}_\perp^2)$ TMDs are plotted with respect to \mathbf{k}_\perp^2 at $x = 0.5$ (solid thin lines) and 0.6 (solid thick lines) for LFHM at model scale $\mu_{\text{LFHM}}^2 = 0.20$ GeV² for J/ψ (left panel) and Υ (right panel) meson, respectively.

distribution at $k_\perp^2 = 0.1$ GeV² than Υ meson when compared to the difference in other TMDs. The last tensor polarized $f_{1TT}(x, \mathbf{k}_\perp^2)$ TMD is given in Figs. 5(e) and 5(f) which is also symmetric under $x \leftrightarrow (1-x)$. There are two units of OAM transfer from initial to final state of the hadron in this case. An overall factor $1/\sqrt{x(1-x)}$ in LFHM enhance the distributions compared to LFQM TMDs distributions. All the TMDs vanish at the end points

$x \rightarrow \{0, 1\}$ for any value of \mathbf{k}_\perp^2 as mentioned in Refs. [42,46] for heavy vector meson. More details on the study of TMDs with respect to both x and \mathbf{k}_\perp^2 in three-dimensional structure for J/ψ -meson have been presented in Fig. 7 for LFHM and in Fig. 8 for LFQM. Similarly, for the case of Υ -meson results have been presented in Figs. 9 and 10 for LFHM and LFQM respectively. Both the models show similar plots when compared to the BSE model [42]

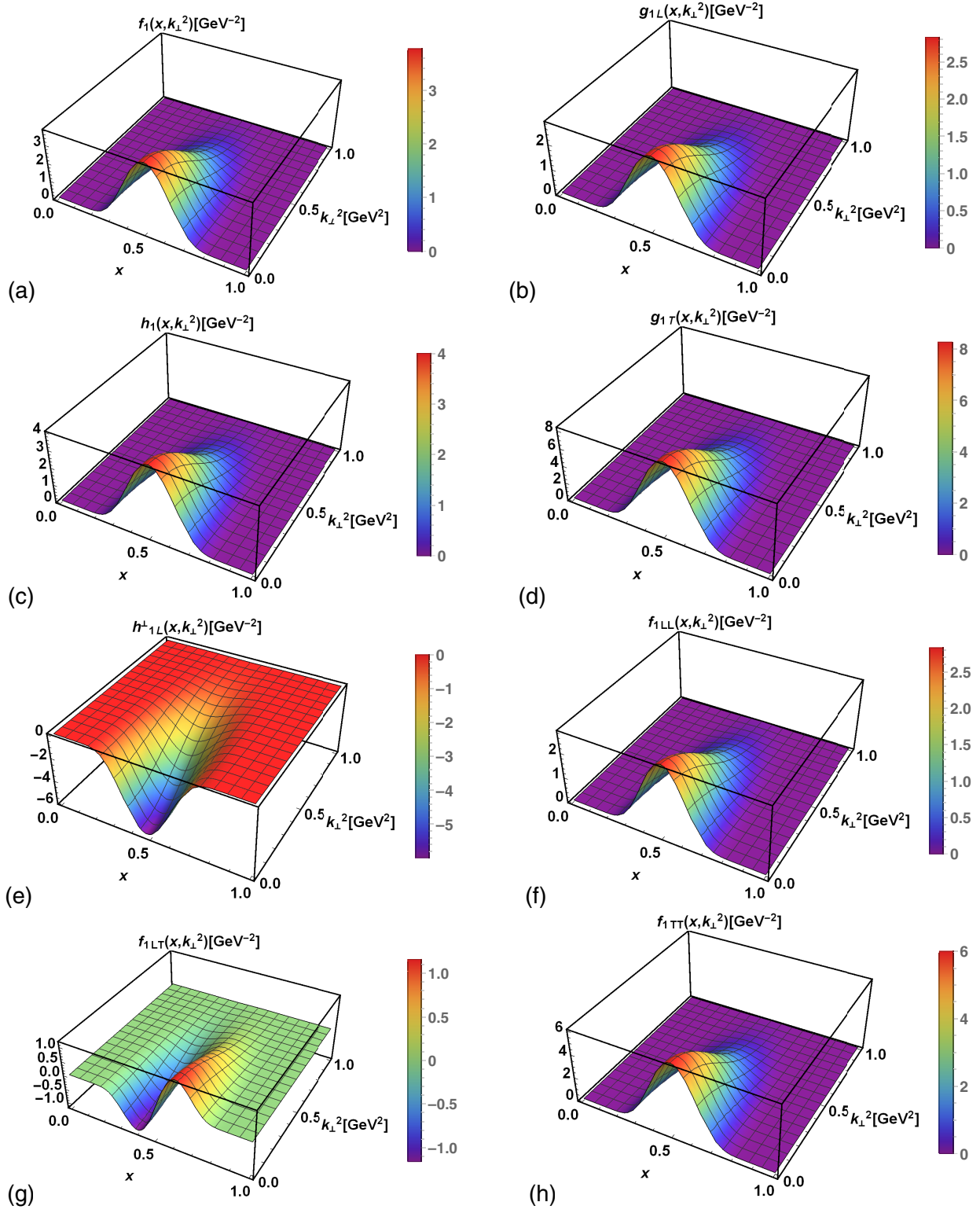


FIG. 7. T -even TMDs for the J/ψ -meson as a function of x and k_{\perp}^2 in the LFHM at the model scale $\mu_{\text{LFHM}}^2 = 0.20 \text{ GeV}^2$.

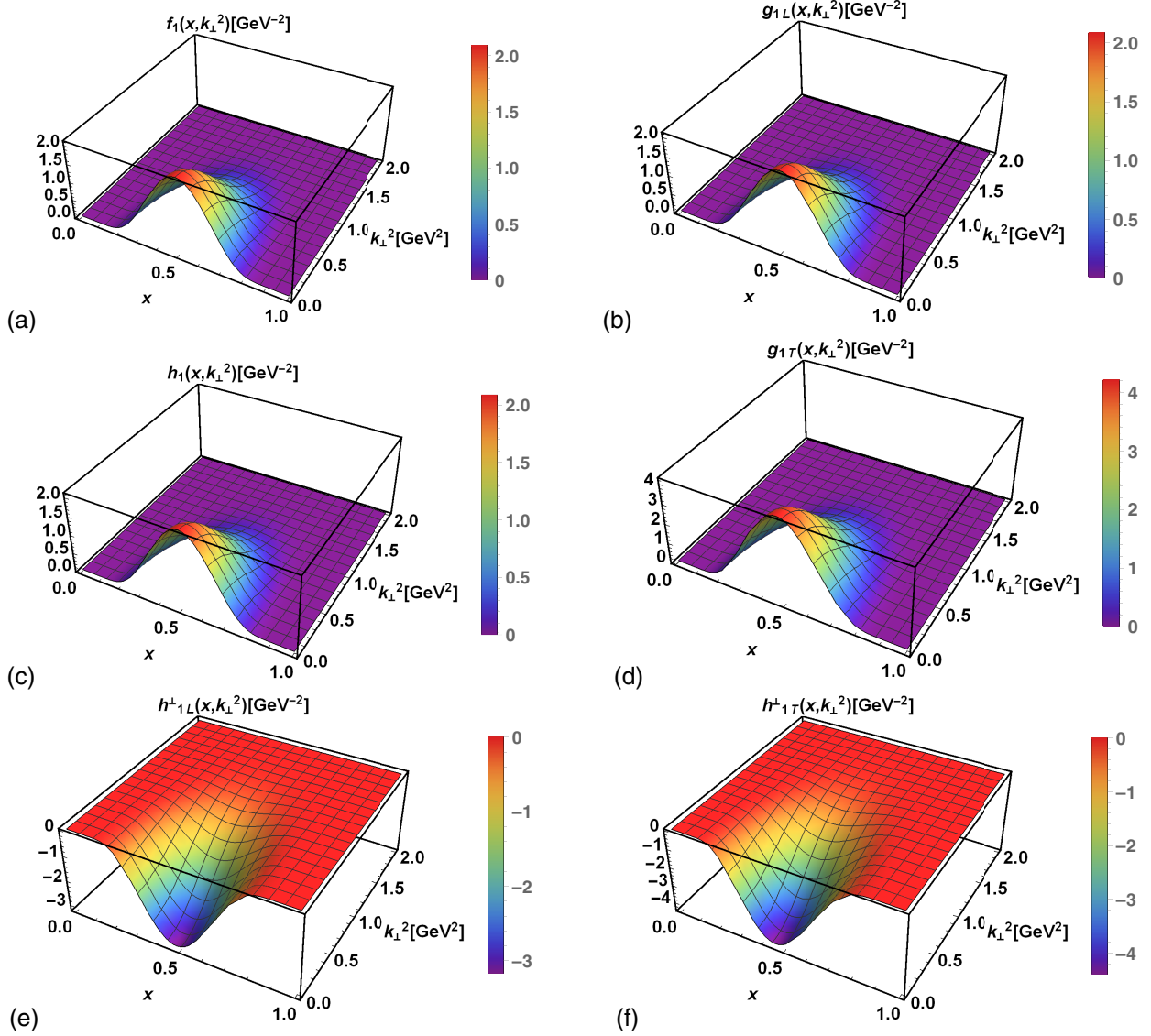


FIG. 8. T -even TMDs of for J/ψ -meson as a function of x and \mathbf{k}_\perp^2 in the LFQM at the model scale $\mu_{\text{LFQM}}^2 = 0.19 \text{ GeV}^2$.

with an exception in the case of J/ψ meson where the BSE model has two different peaks for $f_{1TT}(x, \mathbf{k}_\perp^2)$ TMD as compared to a single peak in our models.

As there is no experimental data available for the case of TMDs to compare our predictions, we have computed average quark transverse momenta $\langle k_\perp \rangle$ for TMDs in both the models for J/ψ and Υ -meson. The average quark transverse momenta $\langle k_\perp \rangle$ is expressed as

$$\langle k_\perp \rangle_{\text{TMD}} \equiv \frac{\int dx d^2\mathbf{k}_\perp |\mathbf{k}_\perp| \text{TMD}(x, \mathbf{k}_\perp^2)}{\int dx d^2\mathbf{k}_\perp \text{TMD}(x, \mathbf{k}_\perp^2)}. \quad (65)$$

In Table I, we have presented our results from LFHM and LFQM and have compared them with the only available theoretical prediction from BSE model [42]. We observe that our results in LFQM for both J/ψ and Υ -meson are

quite similar to the BSE model results. Meanwhile LFHM under estimate the results and are very less as compared to BSE model as well as LFQM. This is true for the case of already computed ρ -meson TMDs as well where the LFHM also gives lower values when compared to NJL model [46] and BSE model [42]. The model input parameters we are choosing for LFHM may be the reason for having lower $\langle k_\perp \rangle$ value as compared to the other models. Since the tensor polarized TMDs for LFQM as well as $h_{1T}^+(x, \mathbf{k}_\perp^2)$ TMD in LFHM are zero, we cannot compute $\langle k_\perp \rangle$ for these TMDs.

III. PARTON DISTRIBUTION FUNCTIONS

PDFs are the distribution functions used to study the one-dimensional internal structure of hadrons [4–7].

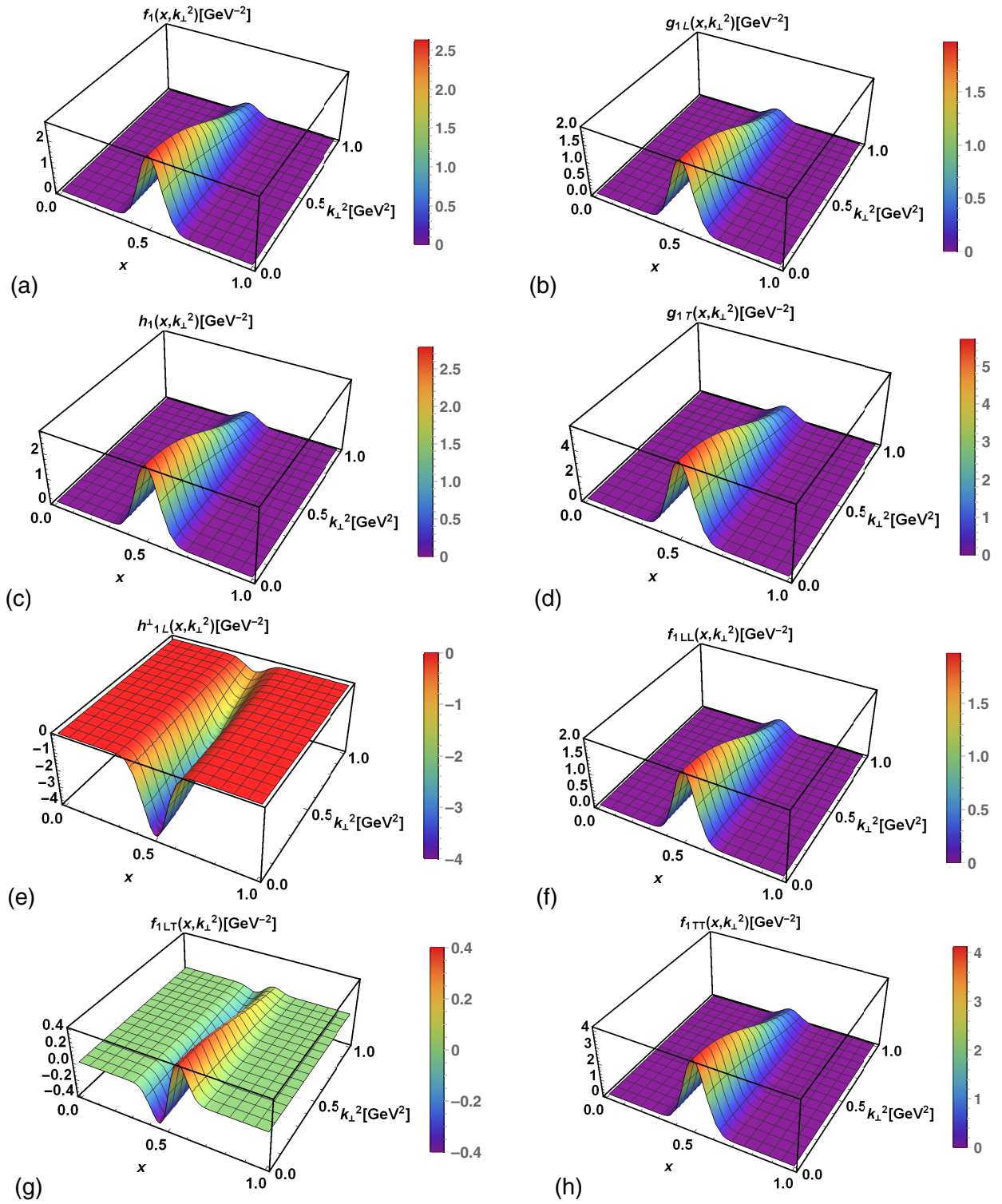


FIG. 9. T -even TMDs for Υ -meson as a function of x and k_{\perp}^2 in the LFHM at the model scale $\mu_{\text{LFHM}}^2 = 0.20 \text{ GeV}^2$.

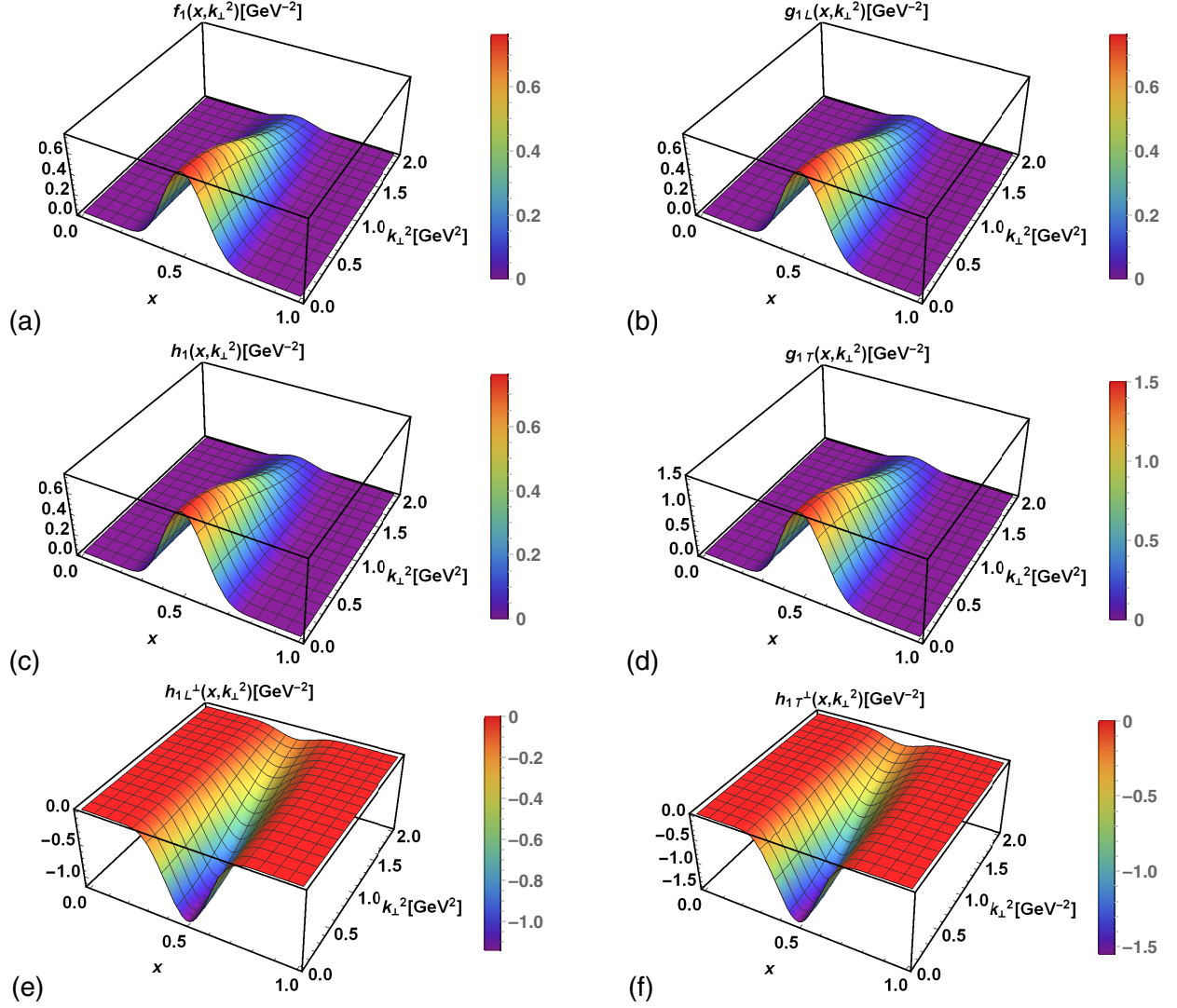


FIG. 10. T -even TMDs of for Υ -meson as a function of x and \mathbf{k}_\perp^2 in the LFQM at the model Scale $\mu_{\text{LFQM}}^2 = 0.19 \text{ GeV}^2$.

TABLE I. The momenta $\langle k_\perp \rangle$ of the LFQM and LFHM compared with the BSE model [42]. The constituent quark masses $m_c = 1.5 \text{ GeV}$ with the AdS/QCD scale $\kappa = 0.894 \text{ GeV}$ for J/ψ -meson and $m_b = 4.63 \text{ GeV}$ with the AdS/QCD scale $\kappa = 1.49 \text{ GeV}$ for Υ -meson in the LFHM, respectively. Similarly, in the LFQM, the values of the parameters are $m_c = 1.68 \text{ GeV}$ with $\beta = 0.699 \text{ GeV}$ for J/ψ -meson and $m_b = 5.10 \text{ GeV}$ with $\beta = 1.376 \text{ GeV}$ for Υ -meson respectively.

TMDs	LFQM		LFHM		BSE model	
	$\langle k_\perp \rangle^{J/\psi}$	$\langle k_\perp \rangle^\Upsilon$	$\langle k_\perp \rangle^{J/\psi}$	$\langle k_\perp \rangle^\Upsilon$	$\langle k_\perp \rangle^{J/\psi}$	$\langle k_\perp \rangle^\Upsilon$
$f_1(x, \mathbf{k}_\perp^2)$	0.620	1.202	0.408	0.667	0.623	1.020
$g_{1L}(x, \mathbf{k}_\perp^2)$	0.600	1.183	0.388	0.656	0.589	1.003
$g_{1T}(x, \mathbf{k}_\perp^2)$	0.619	1.201	0.411	0.668	0.615	1.020
$h_1(x, \mathbf{k}_\perp^2)$	0.610	1.192	0.403	0.664	0.608	1.012
$h_{1L}^+(x, \mathbf{k}_\perp^2)$	0.622	1.204	0.395	0.660	0.608	1.017
$h_{1T}^+(x, \mathbf{k}_\perp^2)$	0.628	1.210	0.602	1.017
$f_{1LL}(x, \mathbf{k}_\perp^2)$	0.441	0.685
$f_{1LT}(x, \mathbf{k}_\perp^2)$
$f_{1TT}(x, \mathbf{k}_\perp^2)$	0.403	0.664	0.764	1.063

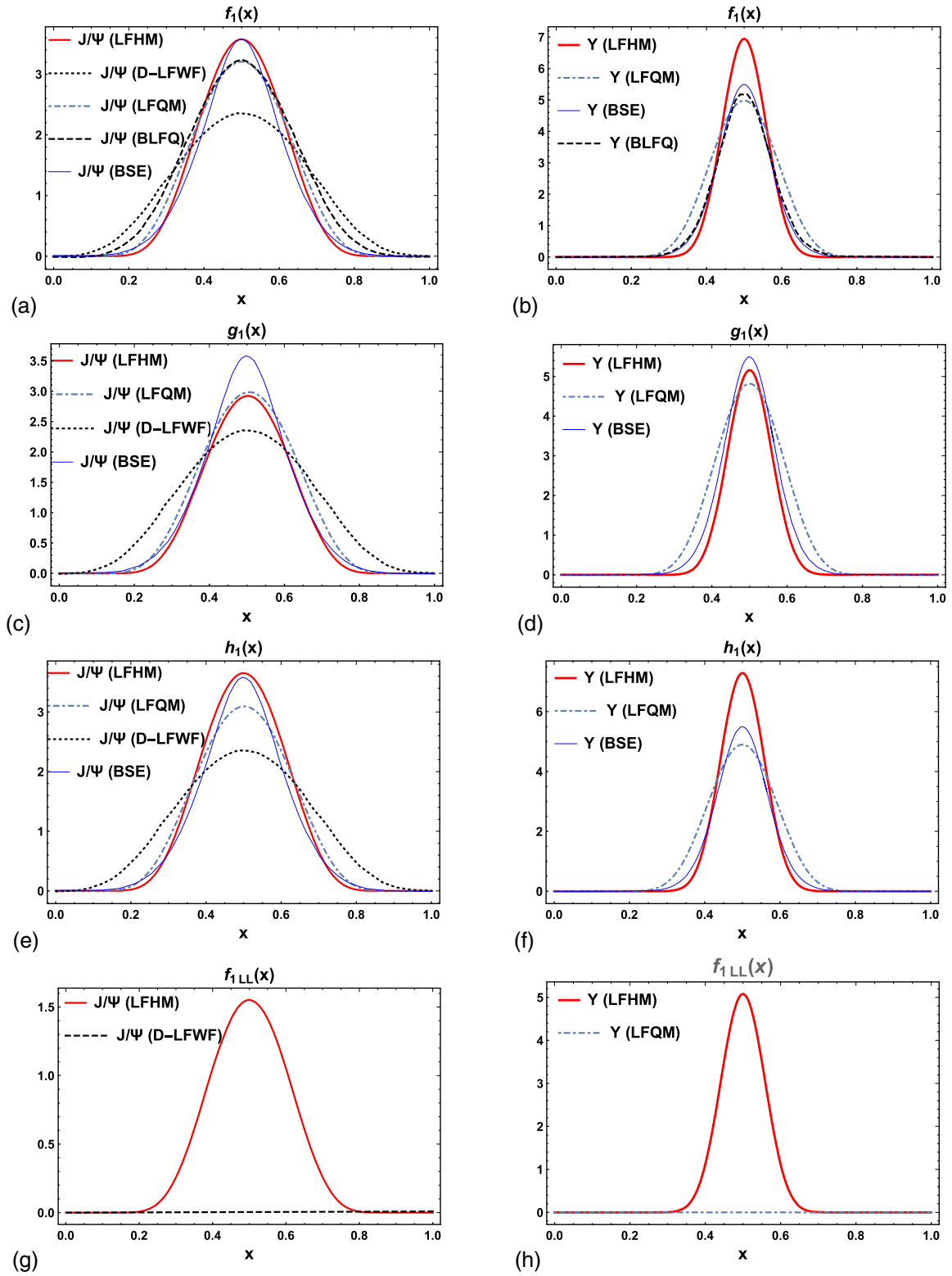


FIG. 11. (a,b) $f_1(x)$, $g_1(x)$, (c,d) $h_1(x)$, and (e,f) $f_{1LL}(x)$ PDFs are plotted with respect to x in different models. The solid thick red and dot-dashed curves in the left and right panels represent the PDFs for J/ψ and Υ mesons in the LFHM (our work) and LFQM (our work), respectively. The black dotted curves are the results from designed-LFWF [49] for J/ψ -meson. The dashed black curves in the left panel are from BLFQ [48]. The blue thin curves are from BSE model [42].

TABLE II. The quark spin sum $\langle x \rangle$ of all the PDFs for both the particles in both LFHM and LFQM compared with the BSE model [42].

PDFs	LFHM		LFQM		BSE model	
	$\langle x \rangle^{J/\psi}$	$\langle x \rangle^\Upsilon$	$\langle x \rangle^{J/\psi}$	$\langle x \rangle^\Upsilon$	$\langle x \rangle^{J/\psi}$	$\langle x \rangle^\Upsilon$
$f_1(x)$	0.97	1.00	1.00	1.00	1.00	1.00
$g_1(x)$	0.81	0.74	0.93	0.97	0.92	0.98
$h_1(x)$	1.00	1.00	0.97	0.98	0.96	0.99
$f_{1LL}(x)$	0.42	0.73

These functions describes the probability of finding the quarks inside the hadrons as a function of longitudinal momentum fraction x . The description of longitudinal momentum and polarization carried by the quarks inside a hadron is encoded by the PDFs. Even though the PDFs do not carry any information about the transverse momentum distribution, they have a direct connection with the TMDs and can be easily accessed through the DIS experiments [8]. There are total 4 PDFs for the case of spin-1 hadrons, which are $f_1(x)$, $g_1(x)$, $h_1(x)$ and tensor PDF $f_{1LL}(x)$ [64].

There are two ways to calculate these PDFs. The first way is to derive these collinear PDFs by integrating Eqs. (2)–(4) over transverse momentum k_\perp . We have

$$\langle \gamma^+ \rangle_{\mathcal{S}}^{(\Lambda)}(x) \equiv f_1(x) + \mathcal{S}_{LL} f_{1LL}(x), \quad (66)$$

$$\langle \gamma^+ \gamma_5 \rangle_{\mathcal{S}}^{(\Lambda)}(x) \equiv \mathcal{S}_L g_1(x), \quad (67)$$

$$\langle \gamma^+ \gamma^i \gamma_5 \rangle_{\mathcal{S}}^{(\Lambda)}(x) \equiv \mathcal{S}_\perp^i h_1(x). \quad (68)$$

The PDFs can also be derived from the TMDs using

$$\mathcal{H}(x) = \int d\mathbf{k}_\perp^2 \mathcal{H}(x, \mathbf{k}_\perp^2), \quad (69)$$

with $\mathcal{H} = f_1(x)$, $g_1(x)$, $h_1(x)$ and $f_{1LL}(x)$.

In Fig. 11, we have plotted the trend of the unpolarized distribution $f_1(x)$, the transversity distribution $h_1(x)$, the helicity distribution $g_1(x)$ and the tensor $f_{1LL}(x)$ PDFs with respect to the longitudinal momentum fraction x carried by the quark. We have compared our LFHM and LFQM results with the BSE model [42], D-LFWF [49], BLFQ [48] results for both the mesons. Overall, the qualitative behavior of our PDFs is consistent with the predictions of the D-LFWF [49], BLFQ [48] and BSE model [42]. The heavy meson PDFs are narrow around x and centered at $x = 0.5$ for all the models.

The PDFs of our models satisfy the quark sum rules [43,46]

$$\int_0^1 dx f_1(x) = 1, \quad (70)$$

$$\int_0^1 dx x f_1(x) + \int_0^1 dx (1-x) f_1(x) = 1, \quad (71)$$

for both the particles as shown in Table II. The quark spin sum values $\langle x \rangle = \int dx \mathcal{H}(x)$ for all the PDFs are given in Table II. $f_1(x)$, $h_1(x)$ and $g_1(x)$ are all come to close to unity for both the mesons. However, due to relativistic effects, the quark spin sum value for Υ -meson is greater than J/ψ -meson. On the other hand, the quark spin sum for the tensor PDF $f_{1LL}(x)$ comes out to be quite less as compared to other PDFs. This may be due to the higher Fock-state contributions playing an important role in the tensor PDF. A similar observation has been made in the BSE model [42]. The positivity constrains on spin-1 TMDs and PDFs [43,46] are also satisfied in our models.

IV. CONCLUSION

In this work, we have presented the J/ψ and Υ -meson T -even TMDs in the light-front holographic model and the light-front quark model. Both the models have been introduced with an addition of the dynamic spin effects in their LFWFs leading to different spin structure for both the models. We have calculated the TMDs using the helicity amplitudes which are basically the overlap form of LFWFs. The relativistic effect being less for the heavy mesons as compared to light mesons, the distribution function are narrower in longitudinal momentum fraction (x) and wider in transverse momentum (\mathbf{k}_\perp^2) of the quarks when compared to the light mesons case. The P and D-wave contributions are quite small compared to the S-wave resulting in the symmetry of most of the TMDs. We have observed that $f_1(x, \mathbf{k}_\perp^2)$, $g_{1L}(x, \mathbf{k}_\perp^2)$, $g_{1T}(x, \mathbf{k}_\perp^2)$, $h_1(x, \mathbf{k}_\perp^2)$ and $h_{1L}^\perp(x, \mathbf{k}_\perp^2)$ TMDs show similar behavior in both the models for both the mesons. The TMD $h_{1T}(x, \mathbf{k}_\perp^2)$ vanishes in LFHM and shows a negative distribution in LFQM. Similarly, the tensor polarized TMDs $f_{1LL}(x, \mathbf{k}_\perp^2)$, $f_{1LT}(x, \mathbf{k}_\perp^2)$ and $f_{1TT}(x, \mathbf{k}_\perp^2)$ are zero for LFQM and nonzero for LFHM. $f_{1LL}(x, \mathbf{k}_\perp^2)$ and $f_{1TT}(x, \mathbf{k}_\perp^2)$ TMDs

shows positive distribution, whereas $f_{1LT}(x, \mathbf{k}_\perp^2)$ have both positive and negative distributions. All the TMD are quite narrow around $x = 0.5$ in LFHM than the LFQM. The TMDs shows symmetry under $x \leftrightarrow (1-x)$ except $f_{1LT}(x, k_\perp^2)$ TMD. $f_{1LT}(x, k_\perp^2)$ TMD shows anti-symmetry under $x \leftrightarrow (1-x)$. Nevertheless, the predictions of spin-1 TMDs in both the models are consistent with the BSE model [42]. All the TMDs, in our models also satisfy the necessary positivity constraints [43,46]. We have also calculated the first momenta $\langle k_\perp \rangle$ for various TMDs and compared with available BSE model [42] data. We observe that the LFQM results are similar to the BSE model, whereas the LFHM underestimate them which may be due to the interplay of some other subtle nonperturbative effects. Finally, we have calculated the unpolarized $f_1(x)$, the transversity $h_1(x)$, the helicity $g_1(x)$ and the tensor $f_{1LL}(x)$ PDFs for J/ψ and Υ -meson in LFHM as well as in LFQM. We have compared these PDFs with the other available theoretical predictions [42,48,49]. The PDFs in this work agree qualitatively with other models

except the $f_{1LL}(x)$ PDF which is zero in Ref. [49]. We have calculated quark spin sum of these PDFs and the results are more close to unity as compared to other models.

In conclusion, this work can also be extended in future to compute the GPDs with different form factors (FFs) for spin-1 particles and spin asymmetry arising in case of J/ψ -meson. Further, adding a nontrivial gauge link to calculate the T -odd TMDs for spin-1 particles in future would not only complete the study of the associated distributions but will also give a complete structure of hadrons through the future experiments to be conducted in BNL and J-Lab.

ACKNOWLEDGMENTS

H. D. would like to thank the Science and Engineering Research Board, Department of Science and Technology, Government of India through the grant (Ref No. TAR/2021/000157) under Teachers Associateship for Research Excellence (TARE) scheme for financial support.

-
- [1] S. J. Brodsky, H.-C. Pauli, and S. S. Pinsky, Quantum chromodynamics and other field theories on the light cone, *Phys. Rep.* **301**, 299 (1997).
 - [2] Y. Iwasaki, K. Kanaya, S. Sakai, and T. Yoshi, Quark confinement in multi-flavor quantum chromodynamics, *Nucl. Phys.* **B30**, 327 (1993).
 - [3] K. G. Wilson, T. Walhout, A. Harindranath, W. M. Zhang, R. J. Perry, and S. Glazek, Nonperturbative light-front QCD, *Phys. Rev. D* **49**, 6720 (1994).
 - [4] J. C. Collins and D. E. Soper, Parton distribution and decay functions, *Nucl. Phys.* **B194**, 445 (1982).
 - [5] A. D. Martin, R. G. Roberts, W. J. Stirling, and R. S. Thorne, Parton distributions: A new global analysis, *Eur. Phys. J. C* **4**, 463 (1998).
 - [6] M. Gluck, E. Reya, and A. Vogt, Dynamical parton distributions of the proton and small x physics, *Z. Phys.* **C 67**, 433 (1995).
 - [7] M. Gluck, E. Reya, and A. Vogt, Dynamical parton distributions revisited, *Eur. Phys. J. C* **5**, 461 (1998).
 - [8] J. Polchinski and M. J. Strassler, Deep inelastic scattering and gauge/string duality, *J. High Energy Phys.* **05** (2003) 012.
 - [9] M. Diehl, Introduction to GPDs and TMDs, *Eur. Phys. J. A* **52**, 6149 (2016).
 - [10] R. A. Martinez *et al.*, Transverse momentum dependent (TMD) parton distribution functions: Status and prospects, *Acta Phys. Pol. B* **46**, 2501 (2015).
 - [11] D. Boer and P. J. Mulders, Time reversal odd distribution functions in lepton production, *Phys. Rev. D* **57**, 5780 (1998).
 - [12] D. Boer, Investigating the origins of transverse spin asymmetries at RHIC, *Phys. Rev. D* **60**, 014012 (1999).
 - [13] M. Diehl, Generalized parton distributions, *Phys. Rep.* **388**, 41 (2003).
 - [14] M. Garcon, An introduction to the generalized parton distributions, *Eur. Phys. J. A* **18**, 389 (2003).
 - [15] A. V. Belitsky and A. V. Radyushkin, Unraveling hadron structure with generalized parton distributions, *Phys. Rep.* **418**, 1 (2005).
 - [16] X. Ji, Deeply virtual Compton scattering, *Phys. Rev. D* **55**, 7114 (1997).
 - [17] L. Favart, M. Guidal, T. Horn, and P. Kroll, Deeply virtual meson production on the nucleon, *Eur. Phys. J. A* **52**, 16158 (2016).
 - [18] M. Garcon, An introduction to the generalized parton distributions, *Eur. Phys. J. A* **18**, 389 (2003).
 - [19] R. A. Martinez, A. Bacchetta, I. I. Balitsky *et al.*, Transverse momentum dependent (TMD) parton distribution functions: Status and prospects, *Acta Phys. Pol. B* **46**, 2501 (2015).
 - [20] J. P. Ralston and D. E. Soper, Production of dimuons from high-energy polarized proton proton collisions, *Nucl. Phys.* **B152**, 109 (1979).
 - [21] J. T. Donohue and S. A. Gottlieb, Dilepton production from collisions of polarized spin 1/2 hadrons: I. General kinematic analysis, *Phys. Rev. D* **23**, 3577 (1981).
 - [22] R. D. Tangerman and P. J. Mulders, Intrinsic transverse momentum and the polarized Drell-Yan process, *Phys. Rev. D* **51**, 3357 (1995).

- [23] J. Zhou, F. Yuan, and Z.-T. Liang, Transverse momentum dependent quark distributions and polarized Drell-Yan processes, *Phys. Rev. D* **81**, 054008 (2010).
- [24] J. C. Collins, Leading twist single transverse-spin asymmetries: Drell-Yan and deep inelastic scattering, *Phys. Lett. B* **536**, 43 (2002).
- [25] S. J. Brodsky, D. S. Hwang, and I. Schmidt, Final state interactions and single spin asymmetries in semi-inclusive deep inelastic scattering, *Phys. Lett. B* **530**, 99 (2002).
- [26] X.-d. Ji, J.-p. Ma, and F. Yuan, QCD factorization for semi-inclusive deep-inelastic scattering at low transverse momentum, *Phys. Rev. D* **71**, 034005 (2005).
- [27] A. Bacchetta, F. Delcarro, C. Pisano, M. Radici, and A. Signori, Extraction of partonic transverse momentum distributions from semi-inclusive deep-inelastic scattering, Drell-Yan and Z-boson production, *J. High Energy Phys.* **06** (2017) 081.
- [28] J. C. Collins, D. E. Soper, and G. F. Sterman, Transverse momentum distribution in Drell-Yan pair and W and Z boson production, *Nucl. Phys.* **B250**, 199 (1985).
- [29] S. Catani, D. de Florian, G. Ferrera, and M. Grazzini, Vector boson production at hadron colliders: Transverse-momentum resummation and leptonic decay, *J. High Energy Phys.* **12** (2015) 047.
- [30] I. Scimemi and A. Vladimirov, Analysis of vector boson production within TMD factorization, *Eur. Phys. J. C* **78**, 89 (2018).
- [31] B. Pasquini, S. Cazzaniga, and S. Boffi, Transverse momentum dependent parton distributions in a light-cone quark model, *Phys. Rev. D* **78**, 034025 (2008).
- [32] I. C. Cloët, W. Bentz, and A. W. Thomas, Transversity quark distributions in a covariant quark-diquark model, *Phys. Lett. B* **659**, 214 (2008).
- [33] M. Wakamatsu, Transverse momentum distributions of quarks in the nucleon from the chiral quark soliton model, *Phys. Rev. D* **79**, 094028 (2009).
- [34] H. Avakian, A. V. Efremov, P. Schweitzer, and F. Yuan, The transverse momentum dependent distribution functions in the bag model, *Phys. Rev. D* **81**, 074035 (2010).
- [35] P. Hägler, B. U. Musch, J. W. Negele, and A. Schäfer, Intrinsic quark transverse momentum in the nucleon from lattice QCD, *Eur. Phys. Lett.* **88**, 61001 (2009).
- [36] S. Sharma and H. Dahiya, Twist-4 T -even proton TMDs in the light-front quark-diquark model, *Int. J. Mod. Phys. A* **37**, 34 (2022).
- [37] S. Sharma, N. Kumar, and H. Dahiya, Sub-leading twist transverse momentum dependent parton distributions in the light-front quark-diquark model, *Nucl. Phys.* **B992**, 116247 (2023).
- [38] S. Meissner, A. Metz, and M. Schlegel, Generalized parton correlation functions for a spin-1/2 hadron, *J. High Energy Phys.* **08** (2009) 056.
- [39] M. Engelhardt, P. Hägler, B. Musch, J. Negele, and A. Schäfer, Lattice QCD study of the Boer-Mulders effect in a pion, *Phys. Rev. D* **93**, 054501 (2016).
- [40] A. Bacchetta, S. Cotogno, and B. Pasquini, The transverse structure of the pion in momentum space inspired by the AdS/QCD correspondence, *Phys. Lett. B* **771**, 546 (2017).
- [41] X. Wang and Z. Lu, Siverson Asymmetry in the pion induced Drell-Yan process at COMPASS within TMD factorization, *Phys. Rev. D* **97**, 054005 (2018).
- [42] C. Shi, J. Li, M. Li, X. Chen, and W. Jia, Transverse momentum distributions of valence quark in light and heavy vector mesons, *Phys. Rev. D* **106**, 014026 (2022).
- [43] S. Kaur, C. Mondal, and H. Dahiya, Light-front holographic ρ -meson distributions in the momentum space, *J. High Energy Phys.* **01** (2021) 136.
- [44] S. Meissner, A. Metz, M. Schlegel, and K. Goeke, Generalized parton correlation functions for a spin-0 hadron, *J. High Energy Phys.* **08** (2008) 038.
- [45] S. Kumano and Q.-T. Song, TMDs for spin-1 hadrons, *J. Phys. Soc. Jpn. Conf. Proc.* **37**, 020130 (2022).
- [46] Y. Ninomiya, W. Bentz, and I. C. Cloët, Transverse-momentum-dependent quark distribution functions of spin-one targets: Formalism and covariant calculations, *Phys. Rev. C* **96**, 045206 (2017).
- [47] Sreeraj Nair, Chandan Mondal, Xingbo Zhao, Asmita Mukherjee, and James P. Vary, Basis light-front quantization approach to photon, *Phys. Lett. B* **827**, 137005 (2022).
- [48] J. Lan, C. Mondal, M. Li, Y. Li, S. Tang, X. Zhao, and J. P. Vary, Parton distribution functions of heavy mesons on the light front, *Phys. Rev. D* **102**, 014020 (2020).
- [49] M. Li, Y. Li, G. Chen, T. Lappi, and J. P. Vary, Light-front wavefunctions of mesons by design, *Eur. Phys. J. C* **82**, 11 (2022).
- [50] Y. Li, P. Maris, and James P. Vary, Quarkonium as relativistic bound state on the light front, *Phys. Rev. D* **96**, 016022 (2017).
- [51] P. J. O'Donnell, Q. P. Xu, and H. K. K. Tung, Weak decays in the light-front quark model, *Phys. Rev. D* **52**, 3966 (1995).
- [52] F. Cardarelli, E. Pace, G. Salme, and S. Simula, Nucleon and pion electromagnetic form factors in a light-front constituent quark model, *Phys. Lett. B* **357**, 267 (1995).
- [53] I. L. Grach, I. M. Narodetskii, and S. Simula, Weak decay form factors of heavy pseudoscalar mesons within a light-front constituent quark model, *Phys. Lett. B* **385**, 317 (1996).
- [54] N. B. Demchuk, Heavy quark limit in the light front quark model, *J. High Energy Phys.* **08** (1998) 008.
- [55] C.-R. Ji and H.-M. Choi, Electromagnetic structure of the ρ meson in the light-front quark model, *Phys. Rev. D* **70**, 053015 (2004).
- [56] H.-M. Choi, Decay constants and radiative decays of heavy mesons in light-front quark model, *Phys. Rev. D* **75**, 073016 (2007).
- [57] H.-M. Choi, Light-front quark model analysis of heavy meson radiative decays, *J. Korean Phys. Soc.* **53**, 1205 (2008).
- [58] H.-M. Choi and C.-R. Ji, Chiral anomaly and the pion properties in the light-front quark model, *Phys. Rev. D* **102**, 036005 (2020).
- [59] G. F. de Teramond and S. J. Brodsky, Applications of AdS/CFT duality to QCD, *Int. J. Mod. Phys. A* **21**, 762 (2006).
- [60] S. J. Brodsky, F.-G. Cao, and G. F. de Teramond, Meson transition form factors in light-front holographic QCD, *Phys. Rev. D* **84**, 075012 (2011).

- [61] S. J. Brodsky and G. F. de Teramond, Light-front holography, light-front wavefunctions, and novel QCD phenomena, *Few-Body Syst.* **52**, 203 (2012).
- [62] A. Bacchetta and P. J. Mulders, Deep inelastic lepton production of spin-one hadrons, *Phys. Rev. D* **62**, 114004 (2000).
- [63] A. Bacchetta and P. J. Mulders, Positivity bounds on spin one distribution and fragmentation functions, *Phys. Lett. B* **518**, 85 (2001).
- [64] S. Hino and S. Kumano, Structure functions in the polarized Drell-Yan processes with spin- $\frac{1}{2}$ and spin-1 hadrons. 2. Parton model, *Phys. Rev. D* **60**, 054018 (1999).
- [65] B. Pasquini and P. Schweitzer, Pion transverse momentum dependent parton distributions in a light-front constituent approach, and the Boer-Mulders effect in the pion-induced Drell-Yan process, *Phys. Rev. D* **90**, 014050 (2014).
- [66] S. Meissner, A. Metz, and K. Goeke, Relations between generalized and transverse momentum dependent parton distributions, *Phys. Rev. D* **76**, 034002 (2007).
- [67] S. J. Brodsky, G. F. de Teramond, H. G. Dosch, and J. Erlich, Light-front holographic QCD and emerging confinement, *Phys. Rep.* **584**, 1 (2015).
- [68] S. J. Brodsky, G. F. de Teramond, and H. G. Dosch, Three-fold complementary approach to holographic QCD, *Phys. Lett. B* **729**, 3 (2014).
- [69] J. R. Forshaw and R. Sandapen, An AdS/QCD holographic wavefunction for the rho meson and diffractive rho meson electroproduction, *Phys. Rev. Lett.* **109**, 081601 (2012).
- [70] R. Swarnkar and D. Chakrabarti, Meson structure in light-front holographic QCD, *Phys. Rev. D* **92**, 074023 (2015).
- [71] M. Nielsen, S. J. Brodsky, G. F. de Teramond, H. G. Dosch, F. S. Navarra, and L. Zou, Supersymmetry in the double-heavy hadronic spectrum, *Phys. Rev. D* **98**, 034002 (2018).
- [72] S. J. Brodsky and G. F. de Teramond, AdS/CFT and light-front QCD, *Subnucl. Ser.* **45**, 139 (2009).
- [73] S. S. Chabysheva and J. R. Hiller, Dynamical model for longitudinal wave functions in light-front holographic QCD, *Ann. Phys. (Amsterdam)* **337**, 143 (2013).
- [74] M. Ahmady and R. Sandapen, Predicting $B^- \rightarrow \rho\gamma$ and $B^-s \rightarrow \rho\gamma$ using holographic AdS/QCD distribution amplitudes for the ρ meson, *Phys. Rev. D* **87**, 054013 (2013).
- [75] M. Ahmady and R. Sandapen, Predicting the isospin asymmetry in $B^- \rightarrow K^*\gamma$ using holographic AdS/QCD distribution amplitudes for the K^* , *Phys. Rev. D* **88**, 014042 (2013).
- [76] M. Ahmady, R. Campbell, S. Lord, and R. Sandapen, Predicting the $B \rightarrow \rho$ form factors using AdS/QCD distribution amplitudes for the ρ meson, *Phys. Rev. D* **88**, 074031 (2013).
- [77] M. R. Ahmady, S. Lord, and R. Sandapen, Isospin asymmetry in $B \rightarrow K^*\mu^+\mu^-$ using AdS/QCD, *Phys. Rev. D* **90**, 074010 (2014).
- [78] M. Ahmady, S. Kaur, C. Mondal, and R. Sandapen, Light-front holographic radiative transition form factors for light mesons, *Phys. Rev. D* **102**, 034021 (2020).
- [79] J.-h. Yu, B.-W. Xiao, and B.-Q. Ma, Space-like and time-like pion-rho transition form factors in the light-cone formalism, *J. Phys. G* **34**, 1845 (2007).
- [80] W. Qian and B.-Q. Ma, Vector meson $\omega - \phi$ mixing and their form factors in light-cone quark model, *Phys. Rev. D* **78**, 074002 (2008).
- [81] S. J. Brodsky, T. Huang, and G. P. Lepage, in *Quarks and Nuclear Forces*, edited by D. Fries and B. Zeitnitz, Springer Tracts in Modern Physics Vol. 100 (Springer, New York, 1982); S. J. Brodsky, T. Huang, and G. P. Lepage, in *Particles and Fields-2*, edited by A. Z. Capri and A. N. Kamal (Plenum, New York, 1983), p. 143.
- [82] T. Huang, B.-Q. Ma, and Q.-X. Shen, Analysis of the pion wave function in the light-cone formalism, *Phys. Rev. D* **49**, 1490 (1994).
- [83] A. J. Arifi, H.-M. Choi, C.-R. Ji, and Y. Oh, Mixing effects on $1S$ and $2S$ state heavy mesons in the light-front quark model, *Phys. Rev. D* **106**, 014009 (2022).
- [84] F. Lu, H.-W. Ke, X.-H. Liu, and Y.-L. Shi, Study on the weak decay between two heavy baryons $B_i(\frac{1}{2}^+) \rightarrow B_f(\frac{3}{2}^+)$ in the light-front quark model, *Eur. Phys. J. C* **83**, 11572 (2023).
- [85] H.-W. Ke, F. Lu, X.-H. Liu, and X.-Q. Li, Study on $\Xi_{cc} \rightarrow \Xi_c$ and $\Xi_{cc} \rightarrow \Xi'_c$ weak decays in the light-front quark model, *Eur. Phys. J. C* **80** (2020).
- [86] Q. Chang, L.-T. Wang, and X.-N. Li, Form factors of $V' \rightarrow V''$ transition within the light-front quark models, *J. High Energy Phys.* **12** (2019) 102.
- [87] H.-M. Choi, H.-Y. Ryu, and C.-R. Ji, The doubly virtual $(\pi^0, \eta, \eta') \rightarrow \gamma^*\gamma^*$ transition form factors in the light-front quark model, *Phys. Rev. D* **99**, 076012 (2019).
- [88] A. J. A. Parada, T. P. Hutaeruk, and K. Tsushima, In-medium properties of the light and heavy-light mesons in a light-front quark model, *Phys. Rev. D* **107**, 114010 (2023).
- [89] W. Wang and Z.-P. Xing, Weak decays of triply heavy baryons in light front approach, *Phys. Lett. B* **834**, 137402 (2022).
- [90] H.-Y. Cheng, C.-W. Chiang, and Z.-Q. Zhang, Two- and three-body hadronic decays of charmed mesons involving a tensor meson, *Phys. Rev. D* **105**, 093006 (2022).